OXIDATION STUDIES
IN
METAL-CARBON SYSTEMS

by

Watt Wetmore Webb

S.B. Massachusetts Institute of Technology 1947

Submitted in Partial Fulfillment of the
Requirements for the Degree of
Doctor of Science
from the
Massachusetts Institute of Technology
1955

Signature of Author _____
Department of Metallurgy
May 16, 1955

Professors in Charge of Research _____

_____

Chairman, Departmental Committee
on Graduate Students _____

OXIDATION STUDIES IN METAL-CARBON SYSTEMS

By

Watt Wetmore Webb

Submitted to the Department of Metallurgy on May 16, 1955

in Partial Fulfillment of the Requirements for the Degree of

Doctor of Science

ABSTRACT

A theoretical analysis of the behavior of carbon during the high temperature oxidation of metal-carbon alloys indicates that in some systems carbon oxides may be evolved at the alloy-oxide interface preventing the formation of a protective metal oxide while in other systems carbon may diffuse away from the interface permitting retention of a protective metal oxide layer. Criteria for predicting behavior in limiting cases have been established.

Oxidation experiments in the systems manganese-carbon, nickel-carbon, tungsten-carbon and titanium-carbon confirmed the theoretical analysis and contributed to the understanding of oxidation of these systems.

An auxilliary investigation into the oxidation kinetics of tungsten between 700 and 1000°C revealed the presence of two conjugated oxide layers only one of which is protective. A mathematical formulation of the oxidation kinetics was worked out and found to agree with the experimental data. Initially the oxidation rate is proportional to the inverse square root of the reaction time but as the reaction progresse the rate approaches a constant value and the protective oxide layer approaches a constant thickness.

Thesis Supervisors: Carl Wagner
John T. Norton
Professors of Metallurgy

TABLE OF CONTENTS

		Page Number
Abstract		ii
Table of Contents		iii
List of Illustrations		v
List of Tables		vii
Acknowledgements		viii
I	Introduction	1
	A. Problem	1
	B. Program	2
II	Experimental Procedures	5
	A. Introduction	5
	B. Preparation of Materials	5
	C. Measurement of Oxidation Kinetics	7
	D. Examination of Reaction Products	12
III	Oxidation of Tungsten	16
	A. Introduction	16
	B. Experimental Details	18
	C. Rate Measurements	18
	D. Structure of the Oxides	20
	E. Summary of the Data	24
	F. Mechanism	27
	G. General Discussion	33
IV	Oxidation Theory for Metal-Carbon Systems	47
	A. Theoretical Analysis	47

		Page Number
	B. Calculation of Carbon Oxide Pressures . .	60
V	Experimental Studies of Metal-Carbon System .	62
	A. Method of Data Presentation	62
	B. Tungsten Carbide	65
	C. Nickel-Carbon System	71
	D. Manganese-Carbon System	78
	E. Titanium-Carbon System	87
	F. Titanium Carbide Based Commercial Hard Metals	96
VI	Recapitulation	107
	A. Conclusions	107
	B. Status of the Problem	108
Bibliography		110
Appendix I	Superheating of Oxidation Samples. .	116
Appendix II	Crystallography of the Oxides of Tungsten	120
Appendix III	Thermal Data for the Oxides of Tungsten	121
Appendix IV	Diffusion of Carbon During Oxidation of Nickel-Carbon Alloys	128
Biographical Note		---

LIST OF FIGURES

Figure Number		Page Number
1	Schematic Diagram of Oxidation Apparatus	14
2	Oxidation Furnace	15
3	Data on the Oxidation of Tungsten	38
4	Linear Plot of Rate Data on the Oxidation of Tungsten	39
5	Linear Plot of Rate Data on the Oxidation of Tungsten	40
6	Photographs of Oxidized Tungsten	41
7	Photomicrographs of Oxidized Tungsten . . .	42
8	Arrhenius Plot of Limiting Parabolic Rate Constants for the Oxidation of Tungsten . .	43
9	Arrhenius Plot of Linear Limiting Rate Constants for the Oxidation of Tungsten	44
10	Expression of the Equation $\frac{b}{a} y + \ln (1 - \frac{b}{a} y) = - \frac{b^2}{a} t$	45
11	Comparison of Theory with Data on the Oxidation of Tungsten Carbide	46
12	Rationalized Data on the Oxidation of Tungsten Carbide	69
13	Photographs of Oxidized Tungsten Carbide. .	70
14	Photomicrographs of Nickel-Carbon Alloys. .	76

Figure Number		Page Number
15	Oxidation of Nickel-Carbon Alloys at 1000°C	77
16	Photomicrographs of Manganese-Carbon Alloys	85
17	Oxidation of Manganese and a Manganese-Carbon Alloy	86
18	Rationalized Data on the Oxidation of Titanium-Carbon Alloys	93
19	Photomicrographs of Oxidized Titanium Carbide	94
20	Photographs of Oxidized Titanium Carbides	95
21	Rationalized Data on the Oxidation of TiC Based Hard Metals and Alloys . . .	104
22	Rationalized Data on the Oxidation of (Ta,Nb) Modified TiC Based Hard Metals and Alloys	105
23	Photomicrographs of Oxides on Nickel Bonded TiC	106

LIST OF TABLES

Table Number		Page Number
I	Limiting Rate Constants for the Oxidation of Tungsten	36
II	X-Ray Diffraction Data on the Tungsten Oxides	37
III	Theory of Oxidation Kinetics of Metal-Carbon Systems	59
IV	Decarburization During Oxidation of a Nickel-Carbon Alloy	128

ACKNOWLEDGEMENTS

Profound thanks are due to Professors Carl Wagner and J. T. Norton for their supervision of this research, and for many stimulating discussions which have been the most elucidative factor of the author's graduate training. In particular, most of the theoretical foundations of this work were laid out in July 1953 by Professor Wagner, or were evolved from discussions with him. The problem was suggested jointly by Professors Norton and Wagner.

The American Electro Metal Company supplied some of the specimens and hot pressed others, and Mr. J. C. Redmond of the Kennametal Company supplied some of the commercial hard metals.

Mr. Peter Koros and Mr. Ernest Abrahamson kindly provided equipment and assisted in the melting of alloys. Mr. Charles S. Fletcher of Harvard University polished some of the specimens for metallographic examination, and Mr. Don Guernsey carried out the chemical analyses.

This work was supported for two years by a fellowship grant from the Allegheny Ludlum Steel Company

Gratitude is also due to Page Chapman Webb and Watt Webb III for their patience, sympathy and encouragement during the course of this research.

I. INTRODUCTION

A. Problem

Although the oxidation of pure metals and alloys has been studied for many years, little has been done to understand the oxidation behavior of the extensive and important group of alloys and metallic compounds containing carbon. Many investigators have measured rates of oxidation and examined the oxide structures for carbon containing alloys such as steels and metal-carbide-based hard metals but consideration of the behavior of contained carbon during the oxidation process has been largely speculative or entirely lacking. Since the oxidation rate of metals often depends on the action of the oxide as a protective barrier layer, the possibility of formation of the gaseous carbon oxides might intuitively be expected to have a disturbing influence on this layer and hence possibly affect the overall reaction rate under some circumstances.

It is the object of this investigation to survey the high temperature oxidation kinetics in metal-carbon systems and to establish a theoretical basis for predicting and understanding in a general way the oxidation behavior of carbon in such systems. It is not intended to supply an exhaustive report of diffusion mechanisms, oxides structures, or rate constants for particular systems in any more detail than is required to understand the behavior of carbon in these systems.

B. Program

The experimental measurements of the kinetics of oxidation of solid metals have usually been found to comply with one of several simple rate equations. These have recently been discussed in great detail in the book "Oxidation of Metals and Alloys," by Kubaschewski and Hopkins[28] and are readily available there.

If diffusion through the oxide formed is the rate limiting step of the reaction, then usually the rate of oxidation is inversely proportional to the thickness of the oxide formed and the progress of the reaction may be expressed by the parabolic oxidation law of Pilling and Bedworth[41],

$$\left(\frac{\Delta m}{A}\right)^2 = k_2 t$$

where Δm = weight change of the specimen

A = area of sample

k_2 = parabolic oxidation rate of constant

t = reaction time

Wagner[53] has discussed in detail the theory of parabolic oxidation as a diffusion limited process and has related the rate constant to other measureable properties of the oxide layer. The theory holds wherever either ionic or electronic diffusion through the oxide is the rate limiting step. It is important to note that the general principles of Wagner's theory may also apply to cases where the parabolic rate law

is not observed due to the simultaneous occurrence of other reactions which obscure the nature of the rate limiting step.

If some surface reaction rather than diffusion is the rate limiting step, the progress of the reaction may often be represented by the "linear oxidation law."

$$\frac{\Delta m}{A} = k_1 t$$

where k_1 is the linear oxidation rate constant.
Although the linear rate law is algebraicly simpler than the parabolic law, less is understood generally about the mechanisms involved.

Other oxidation "laws" have been observed, in particular, the "logarithmic law" is quite common in the thin film range and "a" cubic law is occasionally reported to be applicable to various cases.

The present work is concerned primarily with cases where it was suspected that deviations from the simple theory would be encountered due to complications not ordinarily considered in the oxidation laws mentioned above. It is the immediate objective of this research to study some of these deviations.

Based on a preliminary theoretical analysis of the problem by Professor C. Wagner[52] a theoretical analysis of the possible reactions of carbon during the oxidation of compositions in metal carbon systems has been worked out and used to select particular metal-carbon systems representing the various types of behavior expected. Only systems in which

the pure metal is characterized by a protective oxide layer have been considered since only in these cases would significant differences between the oxidation kinetics of the metal-carbon alloys and the pure metal be expected.

The experimental program consists primarily of direct measurement of oxidation rates as a function of reaction time by weighing specimens as they hang in a hot oxygen filled reaction tube and by measuring the evolution of carbon dioxide. In order to understand the results the mechanical and crystallographic structures of the oxides were determined in some detail.

Although the experimental program was intended to survey a variety of systems it developed that in one system, tungsten-carbon, the oxidation kinetics for the unalloyed metal were in doubt so considerable detail was developed for this material. In addition the performance of some commercial bonded metal carbides was studied.

II. EXPERIMENTAL PROCEDURES

A. Introduction

The experiments conducted center around the measurement of oxidation kinetics described in subsection C below. However, to understand the results obtained from these experiments, supplementary information about the nature of the oxides formed and their behavior under controlled conditions is required. The experimental procedures involved in obtaining this information are discussed in subsection D.

B. Preparation of Materials

Surface preparation: Since the preparation of specimen surfaces may influence the course of surface reactions, exploratory tests were made to determine satisfactory methods for the present work. Kubaschewski and Hopkins[28], pages 72-77, give a discussion of this problem. It was anticipated that surface preparation should not be too critical since only thick films were to be studied. Thus only abraded surfaces were used and preliminary experiments were concerned with the degree of smoothness required and the efficiency of cleaning methods. Comparisons of samples of tungsten, titanium and zirconium which had been abraded and cleaned in various ways showed no important differences after normal oxidation times. It was decided to prepare all specimens for measurement of oxidation rates by merely abrading on 120 mesh alumina paper followed by washing in reagent grade acetone. Since it was

observed in some cases that oxidation occurred preferentially at the edges, the length of edge per unit area of specimen was in those cases maintained roughly constant.

Preparation of Pure Metal Carbide Specimens: Since metal carbides of high purity were commercially available only as powder, powder metallurgy techniques were used in the preparation of metal carbide samples. Hot pressing was required to reduce porosity below a level at which internal oxidation occurred. Pressing was carried out by the American Electro Metals Corp. at appropriate temperatures in graphite molds for roughly 10 seconds, that is, until a limiting value of sample density was reached. The resultant apparent densities consistently exceeded 97 per cent.

Preparation of Nickel-Carbon and Manganese-Carbon Alloys: Induction melting in alumina crucibles under a purified argon atmosphere was used to melt nickel-carbon and manganese-carbon alloys. Tank argon was purified by passing over "Ascarite", "Anhydrone" (magnesium perchlorate) and hot magnesium before being passed through the furnace tube. Test specimens were made by withdrawing the molten alloy into "Vicor" glass tubing by suction and allowing the alloy to freeze in the tubing. Temperatures were approximately determined at the time of sampling by optical pyrometer. Smooth, clean surfaces were usually obtained on the samples but they were abraded on 120 mesh alumina paper before oxidation testing as with other samples.

Preparation of Titanium Alloys: Arc melting using a water cooled copper mold, tungsten electrode and purified argon atmosphere was used to form titanium alloy ingots weighing about 100 grams. Argon was purified as above except that titanium sponge was substituted for magnesium chips in the purification train. The furnace was flushed and evacuated repeatedly before melting and a flow of argon maintained while melting. Contamination of the alloy by tungsten was avoided by striking the arc on a tungsten block and operating with an arc length of at least one-half inch. The ingots were inverted and remelted several times to insure uniformity. Shiny, clean surfaces characterized all of the ingots and samples for oxidation testing were prepared by cutting slices from these ingots which were abraded as usual.

C. Measurement of Oxidation Kinetics

Method: Kubaschewski and Hopkins[28] in their Chapter 2 discuss methods of measuring oxidation kinetics in great detail. The method adopted here follows the standard practice of weighing the sample periodically as it hangs in the furnace from an analytical balance. This yields the weight gain as a function of reaction time while the specimen remains at a constant temperature. If all of the oxidation product adheres to the specimen the weight gain is just the amount of oxygen reacted so the amounts of metal consumed and oxide formed may be determined by stoichiometry provided the composition of the

oxide is known. However, if the oxide is not adherent or if one of the oxidation products is gaseous the weight gain does not unambiguously give a measure of the progress of the reaction. For example, in the case of oxidation of tungsten carbide the following overall reaction might apply:

$$WC + \frac{5}{2} O_2 = WO_3 + CO_2$$

To verify this unambiguously the carbon oxides formed must be measured as well as the specimen weight gain. In order to accomplish this the exhaust gases from the oxidation furnace may be passed over "ascarite" (sodium hydroxide on asbestos) where CO_2 is selectively absorbed. If weighing bottles containing the absorbent are changed at intervals, a plot of the amount of CO_2 evolved vs. time may be made. This procedure was followed in the present work and a block diagram of the apparatus constructed for this purpose is shown in Figure 1. It should be noted that gas evolution and weight gain are determined independently on duplicate specimens, the top of the furnace tube being closed up during gas measurement. A few details are worth noting too. It was found that at 700°C much of the carbon oxidized was not converted to CO_2 but appeared rather as CO. Hence the need for the catalyst furnace in the exit gas train. The design of the oxidation furnace tube (shown in Figure 2) includes a sight glass at the bottom through which the specimen can be observed and on which any oxide which might spall from the sample may be seen immediately.

Since the top of the furnace tube is very narrow, to avoid convection currents it was necessary to hang the specimen from fine straight quartz wires. It was possible to measure weight changes with an accuracy of about ± 0.5 mg provided they occurred slowly.

Temperature Control: Temperatures were uniform to within $\pm 1^{\circ}C$ in a hot zone of 2 inches length with normal gas flow and were maintained at the desired temperature well within $\pm 5^{\circ}C$ by a sensitive temperature controller. Control over short periods was easily maintained within $\pm 1.0^{\circ}$ and drift of the control point caused nearly all of the variations over long periods of time. The use of a heavy stainless steel block around the reaction tube increased the thermal inertia of the furnace and greatly facilitated temperature control.

Another thermal factor involved in the measurement of oxidation kinetics is disposal of the heat of reaction as it is evolved. This problem is usually rightly ignored. However, during the early stages of oxidation of a material following the parabolic rate law the rate of heat evolution is likely to be quite high and the heat of formation of the oxide may not be radiated away with sufficient rapidity to permit temperature control. A straight forward approximate analysis of this problem is derived in Appendix I and presented with a typical calculation. This analysis showed that in some cases excessive temperature rises could occur over a short period of time.

To insure that overheating did not lead to greatly accelerated initial oxidation, in the present studies the specimen is hung in a cold zone of the furnace containing pure O_2 and then it is raised into the hot reaction zone of the furnace. Actually with this technique the reaction begins below the temperature intended. Measurements on typical specimens into which had been inserted a fine Pt - Pt + 10 per cent Rh thermocouple showed that the specimens reached temperature within from 30 to 120 seconds and that no overheating occurred. This thermal lag introduces a fixed uncertainty of this order into the measurement of reaction time.

Discussion of Errors: Calculations of the oxidation kinetics data was carried out in a straight forward manner. However there is one factor which should be considered carefully for oxidation in the thick film range. That is the change of the effective sample area as the oxidation process progresses and the metal is consumed. For example, calculations of metal oxide interface-area-change for the tungsten samples studied gave the following interface area changes for various amounts of oxidation of tungsten to WO_3

$\frac{\Delta m}{A_o}$	$\frac{\Delta A}{A_o}$
0.001 gram/cm^2	.05 per cent
0.01 " "	.5 per cent
0.1 " "	4.7 per cent

Sample size assumed = 0.05 x 1 x 4 cm.

A_o = initial area of sample

ΔA = area change

Δm = total weight change

Kinetics measurements were stopped before 5 per cent area change occurred (except in special cases specifically noted) to avoid area corrections since they are difficult to apply unambiguously.

Analysis of weighing errors can be based on the assumption that the error is determined primarily by the reproducibility of individual balance readings which is essentially independent of Δm but is dependent on the rate of weight gain which governs the time available to take a reading of the balance. Calculation shows that the maximum error is due to sample area change (discussed above) for only a few data. The weighing error turns out to be the principal source of measurement error and is essentially a constant for all data. Calculation of weighing error is based on a weighing precision varying from $\pm$ 0.0002 gram to $\pm$0.001 gram depending on the rate of oxidation. Weighing of specimens on an accurate analytical balance before and after each run provided a check on possible cumulative error of the weight change. The discrepancy was invariably negligible.

In weighings of gas absorption bottles the weight changes were read to $\pm$0.0005 gram and were reproducible to $\pm$0.001 gram consistently.

Analysis of results from duplicate runs on apparently identical specimens indicated that usually the overall reproducibility of data was within the error of measurement. However in some cases, particularly where relatively rapid oxidation was involved, somewhat higher deviations occurred. In Figure 5 data from duplicate runs on tungsten indicate the order of reproducibility obtained in this rather unfavorable case.

The problem of reproducibility must be considered carefully where data on gas evolution and specimen weight gain for metal-carbon alloys are taken on separate runs. Fortunately a good check is possible since the total weight change of the specimen used for gas evolution measurements may be compared with the point corresponding to equal reaction time on the weight change curve of the comparison specimen. For the materials tested in the present work, agreement of these values was invariably within the error of measurement. Only in a few cases which are specifically discussed was the reproducibility of data outside of the range of the error of measurement.

D. Examination of Reaction Products

Determination of Oxide Crystal Structures: X-ray diffraction powder patterns were made using CuKα or CrKα radiation and a General Electric proportional counter spectrometer with intensities recorded on a logarithmic scale. Diffracted radiation was passed through a suitable filter to remove Kβ peaks. Results were analyzed by comparison with ASTM Standard

patterns and with published data and in some cases by calculation from reported structures using the usual principles. See, for example. Barrett[1] or Klug and Alexander[27].

Determination of the Mechanical Form of Oxide Layers: Polished cross sections through metal and oxide layers were prepared for microscopic examination with some difficulties. Samples having soft friable oxides adjacent to hard metal layers were prepared by Mr. Charles S. Fletcher at Harvard University by mounting in thermosetting plastic without pressure, and polished by petrographic techniques on castiron and lead laps. Those having harder oxides were prepared at M.I.T. by standard metallographic techniques. Grinding and preliminary polishing of these sections were accomplished using aluminum oxide polishing paper; finish polishing was carried out on broadcloth covered diamond charged polishing wheels.

In order to determine whether observed porosity of some of these oxides was a bulk phenomenon or merely pitting due to polishing, pincnometric density measurements on the oxides were made using glycerene or water as the dense fluid. It was noted that water was slowly absorbed by the porous oxides and this was taken into account by making the measurements in water as rapidly as possible and weighing the specimen in air both before and after submerged weighing to determine how much water had been absorbed in the specimen pores.

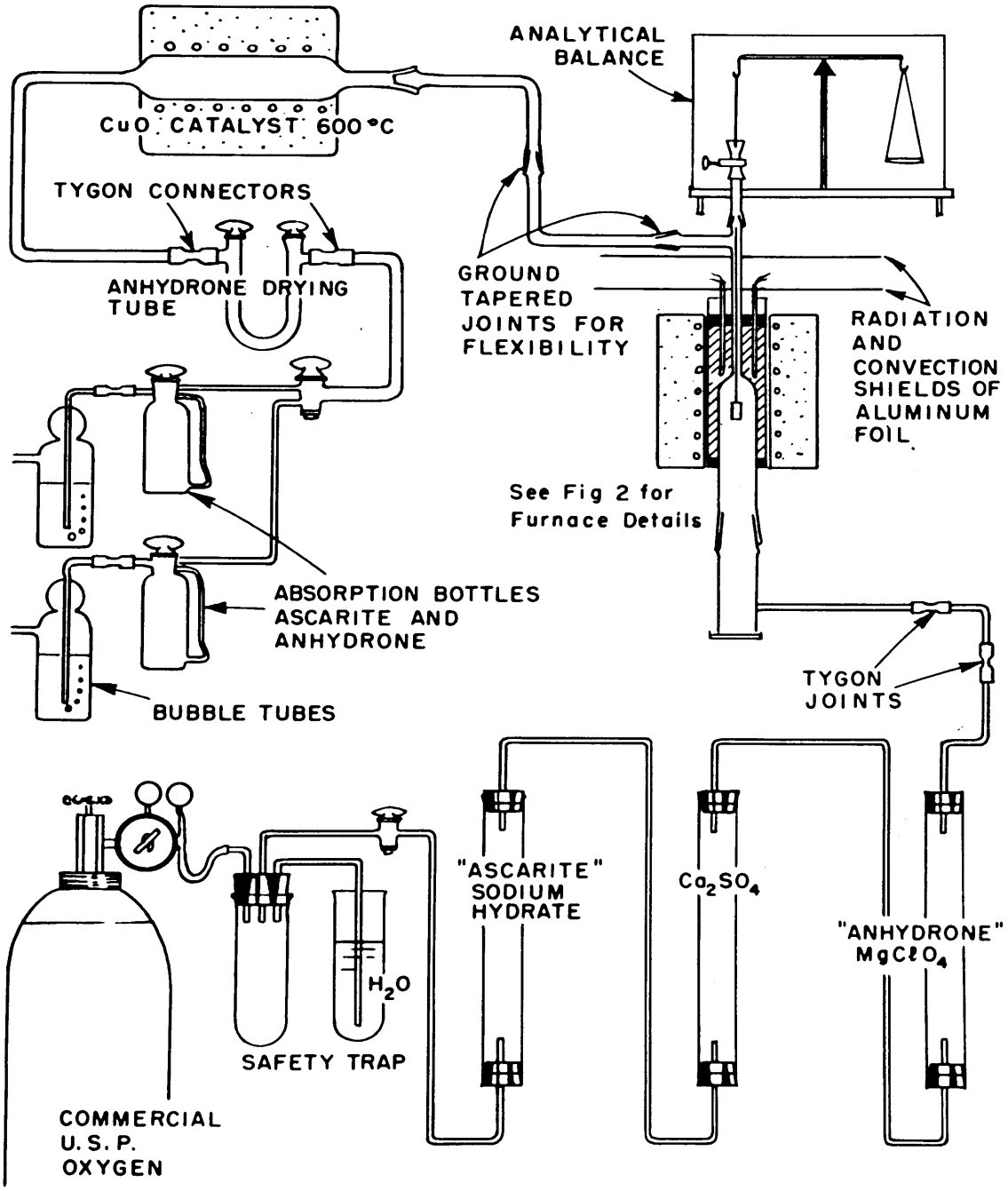

FIG. 1 — SCHEMATIC DIAGRAM OF OXIDATION APPARATUS

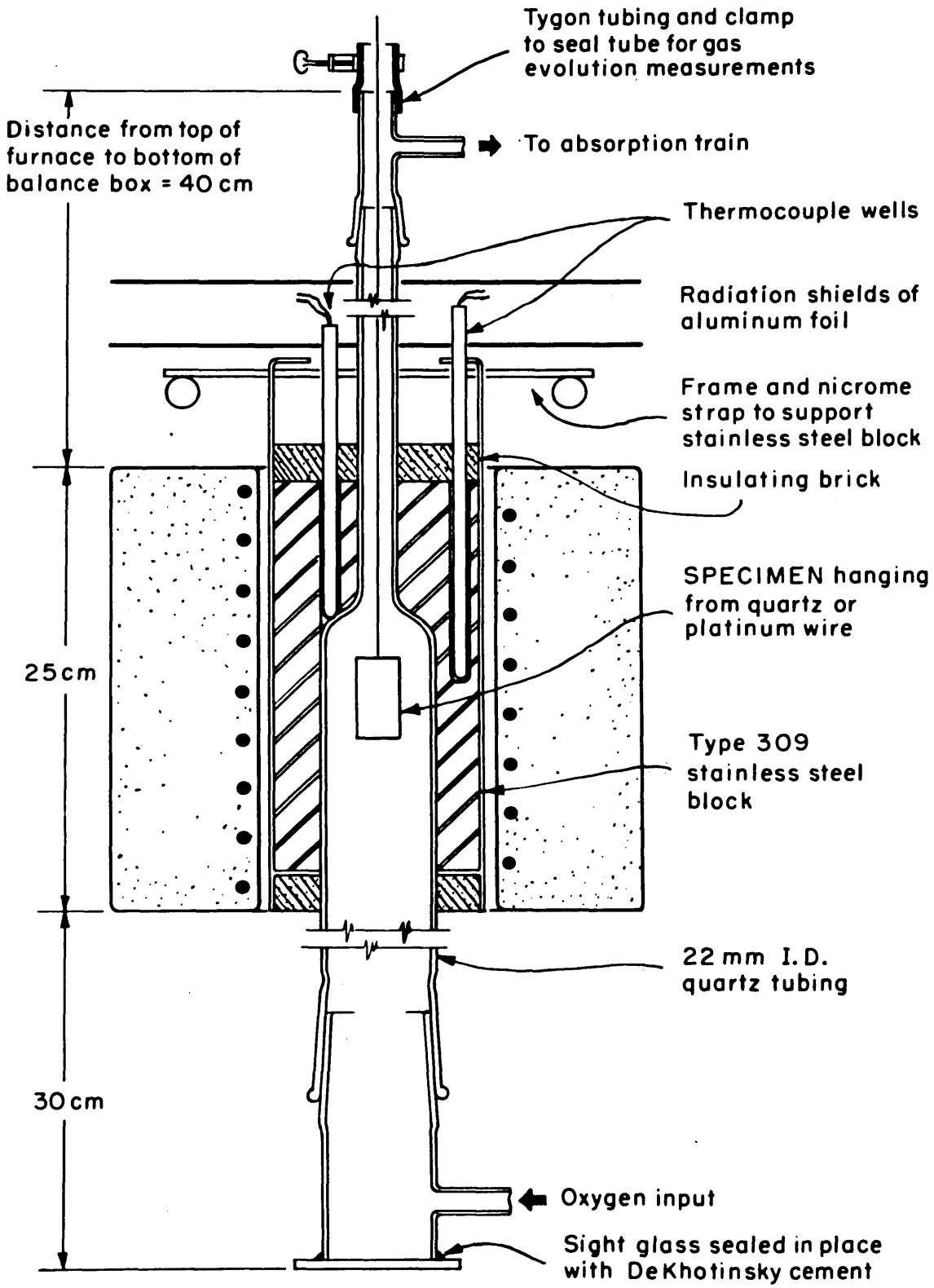

FIG. 2 - OXIDATION FURNACE

III. OXIDATION OF TUNGSTEN

A. Introduction

As a preliminary phase of the studies of oxidation in metal-carbon systems, the oxidation of tungsten was considered in some detail since this case appeared interesting and previous published work was in disagreement.

The oxidation kinetics for tungsten at temperatures above 700°C have been measured by Dunn[10], Scheil[45], Nachtigal[39] and Kieffer and Kolbl[26]. Dunn found a parabolic relationship to hold in the range 700 to 1000°C. On the other hand, Scheil and Kieffer and Kolbl found linear relationships between 500 and 900°C. Nachtigal found that the parabolic rate law applies initially but that later the linear law applied.

Gulbransen and Wysong[15] have studied extensively the behavior of tungsten in oxygen at pressures of 0.1 atmosphere and below in the temperature range 25 to 550°C. They obtained parabolic rate dependence except at .01 atmosphere and 500°C where a linear weight gain was observed. Appreciable volatility of the oxide was noted only under good vacuum at temperatures above 800°C.

The work at temperatures above 500°C thus shows apparent disagreement so present experiments were designed to resolve these discrepancies. It should be noted that while very thick films were formed on the specimens used by Scheil and by Kieffer

and Kolbl during the periods of several days of their tests, the tests of Gulbransen and Wysong and Dunn did not exceed several hours so consequently they formed only relatively thin films.

Millner and Neugebauer[38] in a short article, reported that tungsten tri-oxide is not volatile at 1000°C in O_2 or a vacuum of 1 micron Hg or in argon. However, large amounts of tungsten oxides volatilized in the presence of water vapor in excess of 30 volume per cent.

Hickman and Gulbransen[19] have studied the crystal structures of the oxides formed on tungsten up to 700°C. At all temperatures below 700°C they found only WO_3 but at 700°C both WO_2 and WO_3 were reported, although examination of the diffraction data given suggests that the additional structure observed at 700°C is not necessarily WO_2.

The structures of the various tungsten oxides have been determined by Hägg and co-workers and others and the thermodynamic data on the tungsten oxides has been summarized recently by Coughlin[7]. The crystal structure data are given with references in Appendix II and the thermodynamic data in Appendix III. Recently WO_3 has been investigated at high temperatures due to interest in its reported ferroelectric properties. There appears to be a phase transition at about 740°C and a second order transformation at about 900°C according to Kehl, Hay and Wahl[24] and the investigators quoted by them.

B. Experimental Details

Experimental procedures were described in Section II, and it is necessary to add here only a description of the material used. Tungsten sheet obtained from A. D. McKay Company, (labeled 99.9 per cent pure) 0.5 mm thick was cut into strips ov 5 to 10 cm^2 total area to form the oxidation test specimens. Surface preparation followed the standard method previously described. Chemical analysis of this material showed only the following impurities:

Element	Per cent Impurity	
Fe	0.002	
Si	< 0.005	
Al	0.01	0.01
Ca	< 0.03	
C	0.033	
S	0.004	

C. Rate Measurements

All of the rate data obtained on the oxidation of tungsten are presented graphically in Figure 3 on logarithmic coordinates with the weight gain per unit area in grams per square centimeter plotted against the reaction time in seconds. No allowance is made for the time required for specimens to reach the reaction temperature. Since this is less than 30 seconds in every case, a good idea of the reproducibility of the data may be gained by noting that the systematic deviations between

duplicate runs are about the same magnitude as the error of measurement.

In logarithmic coordinates, data following a parabolic rate law should plot as a straight line with a slope of 0.5 and data following a linear rate law should plot as a straight line with a slop of unity. None of the data observed quite fit a straight line and all of the slopes lie between about 0.5 and 1.0 so that neither a parabolic nor a linear rate law is adequate to represent these results.

Replotting the same data in simple linear coordinates as is done in Figures 4 and 5 shows the trend of the time rate of change of oxidation more clearly. Data points at small oxidation times are omitted for clarity. The oxidation curves start out with a steep slope which gradually decreases until a limiting value is reached beyond which the rate is roughly constant. This suggests that a parabolic rate law may apply for a short time at the beginning of the experiments and that transition to a linear law occurs.

Two experiments under non-standard test conditions were made to determine the effect of certain variations of experimental conditions that appeared critical.

In order to determine whether the reported volatility of WO_3 in the presence of water vapor would affect oxidation rates at pressure of water vapor near that of ambient atmospheric conditions a run was made in oxygen saturated with H_2O at 20°C.

The only significant difference observed was a slight increase in the constant oxidation rate approached after long reaction times. No noticeable deposit of oxide appeared in the furnace.

Since preferred oxidation at sample edges and corners was noticed, specimens with an exceptionally large length of edge per unit of area were oxidized. They showed some irregularities during the early stages of oxidation but only small differences in rate.

Rate constants were obtained from the oxidation data and tabulated in Table I by assuming that initially a parabolic rate law holds and that eventually the linear rate law applies. Rate constants were measured by estimating the limiting values of the slopes of the oxidation curves when suitably plotted. The linear constants are the terminal slopes of data plotted in Figures 4 and 5 and the parabolic constants are the initial slopes of plots of the square of the weight gain per unit area against oxidation time. The range of applicability for each of these approximations is also tabulated in Table I. The criterion for applicability is the absence of systematic deviations from the rate law larger than the maximum error of measurement.

D. Structure of the Oxides

In addition to the measurements of weight gain during oxidation other observations on the mechanical form of the surface oxide were made. The most prominent oxide layer observed had

the chartreuse color typical of WO_3 and was very porous at least after cooling to room temperature. During cooling, about 60 seconds to room temperature, in oxygen the oxide changed from a bright orange to chartreuse. This phenomenon has been reported previously by most investigators of WO_3. The porosity of the yellow oxide was readily ascertained by touching the tip of a fountain pen to the surface which resulted in ink being rapidly absorbed by the oxide. Density measurements indicated that about 30 per cent porosity existed. Photographs of typical oxidized specimens appear in Figure 6 where it can be seen that the extra thick oxide at the edges of the specimens is especially prominent on the heavily oxidized specimen oxidized at 1000°C. A photomicrograph of a cross-section showing the form of the oxides is presented in Figure 7a.

It was observed that the heavy oxide at the edges did not become evident immediately but that it became prominent only in the final portion of the oxidation period. It appeared that oxidation took place more rapidly at the edges so that eventually the metal core of the specimen took on an elliptial rather than rectangular cross-section. However as previously noted, specimens cut to a long narrow shape to provide a larger ratio of edge length to area were observed to approach slightly larger final oxidation rat than others oxidized at the same temperature.

On scraping the yellow oxide from the specimens a hard dark blue layer appeared beneath. This layer adhered tightly

to the metal surface and would not absorb ink placed on its surface. This layer is shown in a photomicrograph taken with an oil immersion objective at 2000X in Figure 7b. The thickness of the blue oxide on this sample is about 4 microns. X-ray diffraction patterns were obtained and its structure and thickness are discussed below. In order to get some idea of its occurrence, tungsten specimens were exposed to the oxidizing atmosphere for just a few minutes at various temperatures. The "blue oxide" invariably appeared and was found to have the same order of magnitude of thickness as those formed under the yellow oxide at longer oxidation times. These specimens also showed an incomplete, thin, powdery layer of yellow oxide over the blue oxide after short exposure times.

Invariably on removal of an oxidized specimen from the furnace the platinum wire which had been tied around it to support it was found outside of the oxide and often fractured by the expansion of the sample during formation of the oxide. This is clear in Figure 6. Outward growth of the yellow oxide from the metal oxide interface was also suggested by the presence on the surface of the oxide of defects present on the original metal surface.

X-ray diffraction patterns of the oxides formed on various specimens were made and some of the data are presented in Table II. Comparison with the ASTM diffraction pattern cards and with results of Gulbransen and Wysong[15] showed numerous

ambiguities due to the large numbers of lines and the complex and rather similar structures of the various tungsten oxides involved. However, using the lattice parameters given by Breakken[3] for α WO_3 a set of "d" values was calculated. All of the lines of all of the patterns obtained from the chartreuse oxide could be fitted quite closely to these "d" values.

By scraping off the chartreuse oxide the blue oxide previously mentioned was exposed on the surface of the metal cores. X-ray diffraction patterns of this oxide on the metal showed strongly the lines of α tungsten and a set of five additional sharp lines which appeared at "d" values which coincided with some of those of WO_3 and of "W_4O_{11}" which is known to have a blue color. However, only the five lines appeared. The d values were consistent with a cubic lattice parameter equal to a multiple of 3.77 Angstroms but relative intensities were not too reproducible and the lack of some of the lines could not be explained from the data obtained. It was possible to chemically remove the blue oxide from the tungsten using concentrated nitric acid and hydrofluoric acid and to obtain a feeble powder pattern from this material by suspending it in thick collodion which was stirred while drying to reduce preferred orientation of the flakes of oxide. No additional lines appeared in this case but the intensities changed significantly.

That the thickness of the blue oxide was less than about 10 microns in every case was shown by a simple calculation of

the maximum X-ray absorption in this layer that would be consistent with the large intensities of the α tungsten diffraction peaks observed from samples having the blue oxide in place on the tungsten substrate.

It should be noted that it was observed that the tungsten sheet used had a rolling texture such that cube poles were roughly perpendicular to the faces of the sheet and that possibly a texture in the blue oxide was indicated by the nature of the lines observed. However an epitaxial relation has not been proven and further work is needed on both the structure and epitaxy of the blue oxide.

E. Summary of the Data

Rates: Although examination of the results for tungsten shows that neither a parabolic or linear law alone is adequate to express the results obtained, it is clear that for relatively short oxidation times the amount of oxidation may be emperically represented by a parabolic equation of the form

$$\left[\frac{\Delta m}{A_o}\right]^2 = k_2 t \qquad (1)$$

where the constant k_2 is given by an Arrhenius equation

$$k_2 = k_{o2} \quad \frac{-Q_2}{RT} \qquad (2)$$

in which the constants were found to have the values: (See Figure 8)

$$\log k_{o2} = 1.5 \pm 1.1 \ (g^2 \ cm^{-4} \ sec^{-1})$$

$$Q_2 = 45{,}000 \pm 6{,}000 \text{ calories}$$

These values check reasonably well with those obtained by calculation from the data of Gulbransen and Wysong[15] and Dunn[10] at temperatures up to 850°C as plotted in Gulbransen and Wysong's Figure 23. Their data yield:

$$\log k_{o2} = 3.6 \ (g^2 \ cm^{-4} \ sec^{-1})$$

$$Q = 52{,}500 \text{ calories}$$

Dunn's data show a substantial deviation from an Arrhenius plot in the range 850 to 900°C which was not considered in detail in the present investigation but there is some evidence of irregularity at 900°C. His results are in general agreement with the present work as can be seen from Figure 8.

The data of both Dunn and Gulbransen and Wysong were taken over sufficiently short oxidation times that the parabolic approximation would be expected to hold. The range over which the parabolic approximation holds may be seen from Table I to correspond to a constant amount of oxide formation. Hence the time period for which the parabolic law may be applied decreases as the temperature (and the oxidation rate) increases.

In the limit of long oxidation times it appears that the amount of oxidation may be represented by a linear equation of the form:

$$\frac{\Delta m}{A_o} = k_1 t + c \qquad (3)$$

where the constant k_1 is given by an Arrhenius equation

$$k_1 = k_{o1} \frac{-Q_1}{RT} \qquad (4)$$

in which the constants were found to have the values: (See Figure 9)

$$\log k_{o1} = 0.5 \pm 0.5 \text{ (g cm}^{-2} \text{ sec}^{-1})$$

$$Q_1 = 30{,}500 \text{ calories} \pm 2{,}500 \text{ calories}$$

The constant c is added to account for the initial period during which the linear equation cannot be applied. These data at long oxidation times are of limited practical value due to the pronounced effect of test conditions on the rates observed. However where conditions were accurately duplicated the data were easily reproducible.

Oxides: The principal oxide found on tungsten was $\alpha - WO_3$ in a porous powdery form with a measured apparent density roughly 70 per cent of the X-ray density regardless of the temperature at which oxidation was carried out. This oxide had a yellow or chartreuse color and appeared from its form to have grown outward from its inner surface rather than having been formed by combination of metal and oxygen atoms at its outer surface. At room temperature, at least, this oxide was porous.

Another oxide of uncertain structure and chemical composition called here the "blue oxide" was found tightly adhering to the tungsten. It did not have a diffraction pattern characteristic of any of the known tungsten oxides but is a distorted

form of one of the higher oxides, probably "W_4O_{11}". However positive identification is not at present possible. It had a maximum thickness of<10 microns and was formed rapidly at the beginning of the oxidation.

F. Mechanism

The rate dependence observed in this case is not uncommon. Transitions from a parabolic to a linear rate law are usually noted in the literature as small deviations from one or the other rate law. However in the present case supplementary observations of the details of occurrence of the oxides suggest a basis for a more quantitative analysis.

It was observed that two oxide layers appeared on tungsten, one, the blue oxide, formed quickly and then did not increase greatly in thickness, and the other, the yellow oxide, α WO_3, appears as an outer porous layer which continues to grow rapidly during the entire oxidation period. Its porosity is sufficient that it probably is not much of a barrier for the passage of oxygen molecules.

Noting that the rate of oxidation during the first stages of oxidation approximates a parabolic rate equation and that this rate is observed before the yellow oxide has formed a complete surface layer, we assume that diffusion through the blue oxide controls its own formation rate. Then noting that the porous yellow oxide forms outside of the blue oxide we assume, on the basis of the discussion of the previous section,

that the yellow oxide forms from the blue oxide process without further oxygen absorption in weighable amounts. We next assume that the rate of transformation of the blue oxide into yellow oxide is constant. This is enough to establish the basis of a general model for a mathematical analysis to which we next proceed.

Mathematical Analysis: Consider the case of the formation of two successive oxide layers on a metal during oxidation where the inner layer is protective so that diffusion through it controls its rate of formation. Then if the outer oxide layer is not protective due to (say) porosity its rate of formation by transformation from the inner layer may be assumed constant. These rates may be expressed in terms of the weight of oxygen per unit area in each layer as follows. Let:

y = amount of oxygen in the barrier layer per unit area at time t

z = amount of oxygen in the outer (porous) layer per unit area at time t.

Then $\frac{dy}{dt} = \frac{a}{y} - b$ (1)

$\frac{dz}{dt} = bf$ (2)

where f is the ratio of the oxygen content per gram atom metal in the outer layer to that in the inner layer and a and b are appropriate constants. These equations have been proposed previously by Lorier[31] for the oxidation of Cerium.

The units of a are $g^2\ cm^{-4}\ sec^{-1}$ and b are $g\ cm^{-2}\ sec^{-1}$. Integration of equations (1) and (2) yield

$$\ln\left[\frac{1}{1-\frac{b}{a}\,y}\right] - \frac{b}{a}\,y = \frac{b^2}{a}\,t \qquad (3)$$

and

$$z = bft \qquad (4)$$

A particular characteristic of this model is that the inner oxide layer reaches a maximum thickness in the limit $t \to \infty$ The limiting value of the weight of oxygen in the inner layer turns out to be

$$y\ (\text{maximum}) = \frac{a}{b} \qquad (5)$$

The over all weight gain per unit area which is often measured in studies of oxydation kinetics may be expressed for this case as:

$$\frac{\Delta m}{A} = y + z \qquad (6)$$

where y and z are functions of t determined by equations (3) and (4).

In order to test the validity of equation (6) it is necessary to obtain a plot of (Δ m/A) against t for comparison with experimental data. This may be done by using equations (3), (4) and (6). First we note that in equation (3) the constants a and b are so arranged that they appear as dimensionless groups with the variables; therefore, equation (3) may be represented graphically in a plot independent of particular

values of a and b. Equation (3) establishes a relation between the dimensionless groups by/a and b^2t/a.

Thus we may plot

$$-\ln\left(1 - \frac{b}{a}y\right) \text{ versus } \frac{b^2}{a}t$$

which is a particularly convenient form as will become apparent.

This has been computed and appears as Figure 10. It should be pointed out that on a logarithmic scale this is very nearly but not quite a straight line. Combining equations (6), (3) and (4) leads to the useful form for the weight gain per unit area,

$$\frac{\Delta m}{A} = -\frac{a}{b}\ln\left(1 - \frac{b}{a}y\right) + b\,(f - 1)\,t \qquad (7)$$

the term $\ln(1 - \frac{b}{a}y)$ can be obtained as a function of t directly from Figure 10 if the values of a and b are known. The significance of the constants a and fb is seen by observing the limits approached by equations (1) and (2):

$$a = \frac{1}{2}\lim_{t\to 0}\frac{d\left[\frac{\Delta m}{A}\right]^2}{dt} \qquad (8)$$

$$fb = \lim_{t\to\infty}\frac{d\left[\frac{\Delta m}{A}\right]}{dt} \qquad (9)$$

The constants a and fb are associated with the parabolic and linear oxidation rate constants by the relations

$$a = \frac{k_2}{2} \qquad (10)$$

$$fb = k_1 \qquad (11)$$

as may be seen by comparison with equations (1) and (2) of Section I.

The relations (10) and (11) may be utilized to obtain the values of a and bf from experimental data at short and long oxidation times if a sufficiently large time range is considered. However, other independent information such as the chemical compositions of the two oxide layers must be known to obtain a value for f independent of b.

Utilizing equation (3) the thickness of the inner oxide layer may be computed as follows:

$$d = \frac{\Delta M}{16X} \frac{1}{\rho} y(t) \qquad (12)$$

where d is the thickness in centimeters, M is the formula weight of the inner oxide, X is the number of oxygen atoms per formula and ρ is the inner oxide density in g cm^{-3}. In the limit as $t \to \infty$ a maximum thickness is approached as is seen from equation (5); namely

$$d(\text{maximum}) = \frac{a}{b} \frac{M}{16X} \frac{1}{\rho} = \frac{k_2 M}{2k_1 16X \rho} \qquad (13)$$

Comparison with Experiment: The oxidation of tungsten in the range 700 - 1000°C appears to be rather well described by this model. If the observed values for k_1 and k_2 are used

and f is approximated by unity (see below), a set of calculated curves of weight gain versus time may be calculated. The results have been plotted along with the measured oxidation curves in Figure 11 where it is seen that the agreement is good even for very small oxidation time where plotting on logarithmic coordinates amplifies the deviations which are about equal to the experimental error. However, the deviations suggest that either there are deviations from this model in the thin film range just as is often observed for cases where the parabolic rate law applies or the values of k_2 are not quite right. At 900°C it appears that there is an additional complication the nature of which is not clear. The calculated maximum thickness according to equation (12), about 5 microns, and rapid initial growth of the inner oxide layer according to equation (13) agree with the observations by micrography and X-ray absorption.

The value of f chosen is not entirely arbitrary since the microscopic observations and X-ray diffraction data give a hint that the inner oxide is probably similar to WO_3 or "W_4O_{11}". The maximum possible range of f in this case is from 1.0 to 1.09. The shape of the calculated oxidation curves is rather insensitive to variation of f within this range, so it remains for an independent determination of the composition of the blue oxide to decide the proper value of f to use for tungsten.

G. General Discussion

It has often been observed during studies of the oxidation of a pure metal that for a portion of the reaction period one of the simple rate laws is followed closely but that eventually there is a transition to a different behavior. This observation has been discussed in the literature and many specific cases have been clarified. In particular it has been observed that quite often a parabolic rate law applies initially but eventually there are deviations until it becomes evident that there has been a transition to a constant oxidation rate, that is, to a linear rate law. It has been shown above that tungsten shows this behavior.

Evans[12] has suggested that practically any irregular rate dependence during oxidation, including the transition from a parabolic to a linear rate law may be explained by formation of blisters, flakes, or fissures in the oxide leading to accelerated and irregular oxidation. Following Evans' suggestion one assumes a suitable rate of formation of mechanical defects in the oxide, notes that in real cases measurements of oxidation kinetics yield only an average rate over all parts of the specimen and thus transition behavior of any form is explained. Undoubtedly this approach explains the results observed in some cases in the literature.

On the other hand there are data in the literature for cases where the transition of rate law occurs where more than

one oxide is formed. One oxide may be a dense protective oxide and the other may tend to form in a porous powdery layer. In particular, Loriers[31] has reported this for cerium at temperatures around 60°C and his results have been confirmed by Cubicciotti[8] up to 125°C. Here the two oxides occurring are Ce_2O_3 which is dense and CeO_2 which is porous. Loriers[32] has also found this transition behavior and two oxide layers, one porous and one non-porous on uranium at temperatures between 140 and 240°C. Similar transition from a parabolic to a linear rate law have been reported for a number of other metals but in most cases the nature of the oxides occurring is not certain and other complications appear.

In the present research a detailed mathematical description has been worked out for transition behavior due to formation of two oxides one of which is porous, and the results have been compared with the observations on tungsten. It is probable that this mathematical description applies to these other cases too. Loriers[39] has previously suggested the essentials of this mathematical analysis in discussing the data on cerium. He has also suggested that the reason the outer oxide becomes porous is that its specific volume (per mole of metal) is less than that of the underlying porosity-free oxide. Whether this is true for tungsten is not clear due to the difficulty of identifying the underlying oxide with real certainty.

The oxidation of tungsten seems to be rather more complex than either Scheil or Dunn anticipated although the data obtained in the present work is in good agreement with theirs. In the limit of long oxidation times Scheil's conclusion that a constant rate is reached is correct and in the limit of short oxidation times Dunn's conclusions that the parabolic rate law holds is correct. However, it appears that diffusion through the inner blue oxide is the rate limiting step in the reaction and the transformation of this oxide into the yellow oxide leads to the special rate law derived here.

TABLE I

Limiting Rate Constants for the Oxidation of Tungsten

		Parabolic Approximation		Linear Approximation		
Temp. °C	Run No.	K_2 $\frac{g^2}{cm^4 sec}$	Max Range $\frac{\Delta m}{A_o}$	K_1 $\frac{g}{cm\ sec}$	Min $\frac{\Delta m}{A_o}$	Max $\frac{\Delta m}{A_o}$
700	6	2.5×10^{-9}	20×10^{-4}	3.9×10^{-7}	150×10^{-4}	500×10^{-4}
700	7	Irregular	-	3.9×10^{-7}	150×10^{-4}	500×10^{-4}
700	8*	2.5×10^{-9}	20×10^{-4}	5.6×10^{-7}	45×10^{-4}	400×10^{-4}
700	14**	Irregular	-	4.3×10^{-7}	125×10^{-4}	425×10^{-4}
800	9	3.0×10^{-8}	50×10^{-4}	3.2×10^{-6}	100×10^{-4}	500×10^{-4}
800	16	3.0×10^{-8}	50×10^{-4}	3.0×10^{-6}	100×10^{-4}	500×10^{-4}
900	10	1.0×10^{-7}	150×10^{-4}	5.75×10^{-6}	200×10^{-4}	300×10^{-4}
900	12**	1.3×10^{-7}	160×10^{-4}	7.5×10^{-6}	(irregularities)	
1000	11	7.3×10^{-7}	220×10^{-4}	1.8×10^{-5}	150×10^{-4}	650×10^{-4}
1000	13	7.3×10^{-7}	220×10^{-4}	1.8×10^{-5}	350×10^{-4}	800×10^{-4}

* Oxidized in O_2 saturated with H_2O at 23°C

** Large edge-to-area ratio

TABLE II

X-ray Diffraction Data on the Tungsten Oxides

Tungsten		Calculated for WO_3*		Yellow Oxide Observed	"Blue Oxide" Observed	Blue Oxide W_4O_{11} reported**	Calculated for assumed cubic a_o = 3.77	
Indices	d Values	Indices	d	d	d	d	Indices	d
		010	7.48					
		100	7.28			3.917		
		010	5.22					
		001	3.82	3.84				
		020	3.74	3.77	3.77	3.779	(100)	3.77
		200	3.64	3.66		3.625		
		011	3.40					
		101	3.38					
		120	3.33	3.35				
		210	3.22					
		111	3.09	3.10				
		021	2.67	2.70		2.737		
		201	2.63	2.63	(2.63)	2.621	(110)	2.63
		220	2.61					
		121	2.52	2.52				
		212	2.51					
		211	2.49					
		030	2.46					
		300	2.43			2.442		
		130	2.36					
		310	2.31					
110	2.23	221	2.16	2.16		2.216	(111)	2.16
		031	2.09					
		230	2.06					
		301	2.05					
		320	2.04	1.92 broad				
		131	2.01					
		331	1.95					
		040	1.87	1.88	1.88	1.975	(200)	1.88
		012	1.85			1.845		
111	1.83	102	1.84					
		400	1.82					
		231	1.81					
		321	1.80					
		112	1.79					
		330	1.74	1.71		1.750		
		022	1.70	to		1.700		
		202	1.69	1.65	(1.68)	1.674	(210)	1.68
200	1.58	331	1.58			1.552		
		222	1.54	1.56		1.525	(211)	1.53
		032	1.51	to		1.455		
				1.46		1.339		
						1.286	(220)	1.31
211	1.29				1.26	1.261	(300)	1.26
220	1.12					1.207		
310	0.993							
		080	0.937	0.94				
222	0.913							

* Values for WO_3 approximated by assuming orthorhombic rather than lattice which is justified by the small difference in this case.

** ASTM Data Card II 711.

NOTE: d values underlined were the strongest lines.

All d values in Angstrom Units.

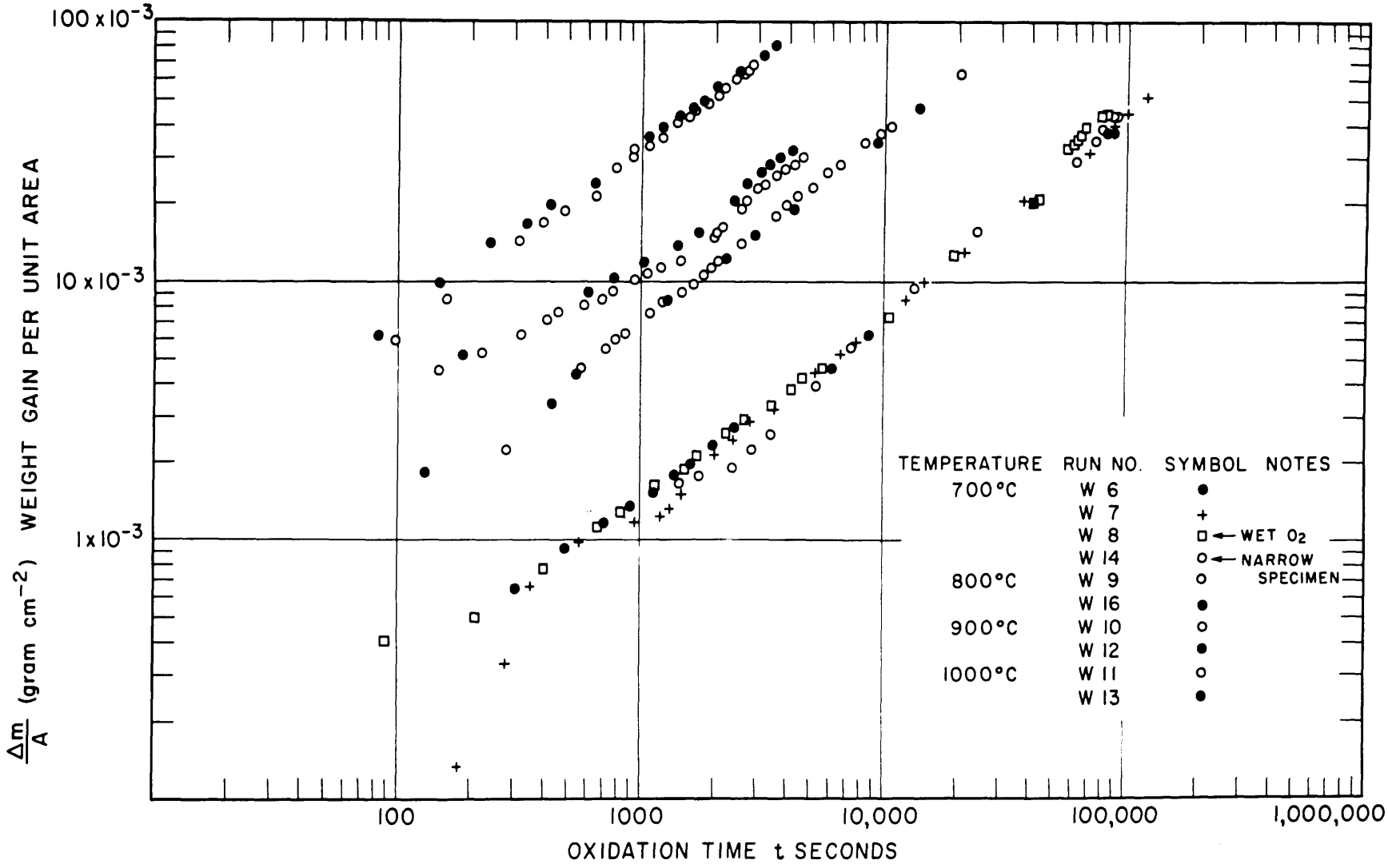

FIG. 3 - DATA ON THE OXIDATION OF TUNGSTEN

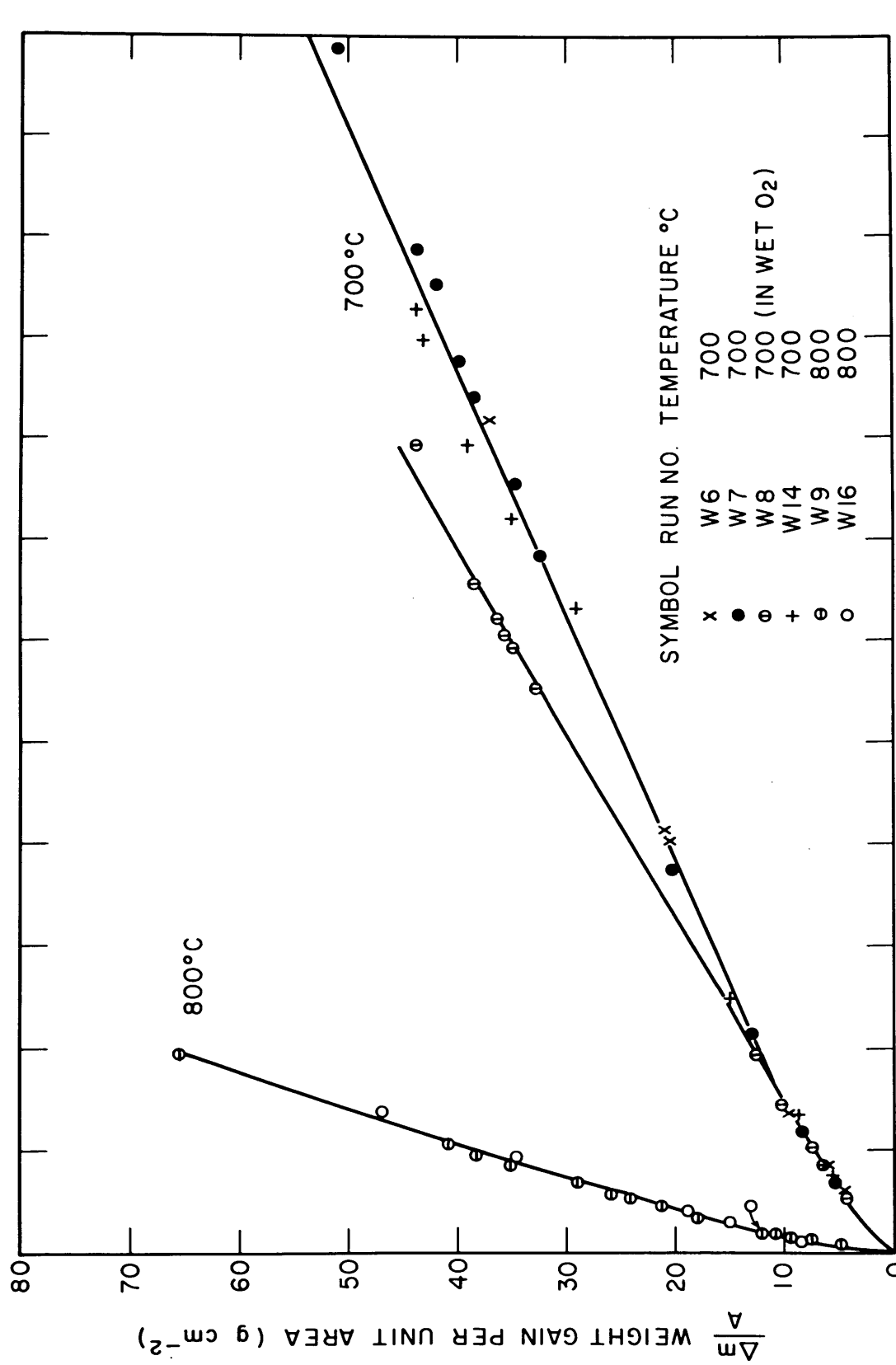

FIG. 4 - LINEAR PLOT OF RATE DATA ON THE OXIDATION OF TUNGSTEN

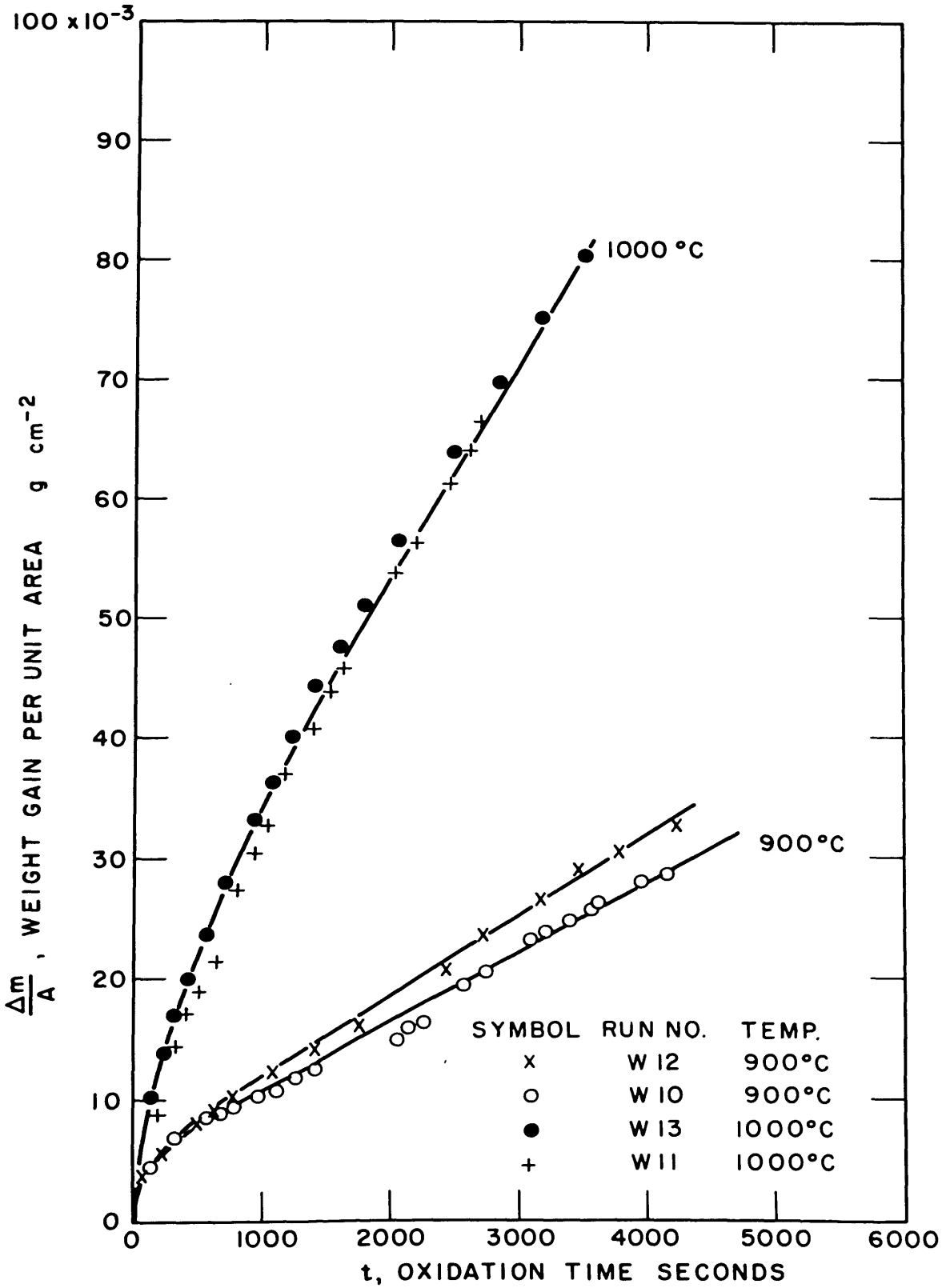

FIG. 5 - LINEAR PLOT OF RATE DATA ON THE OXIDATION OF TUNGSTEN

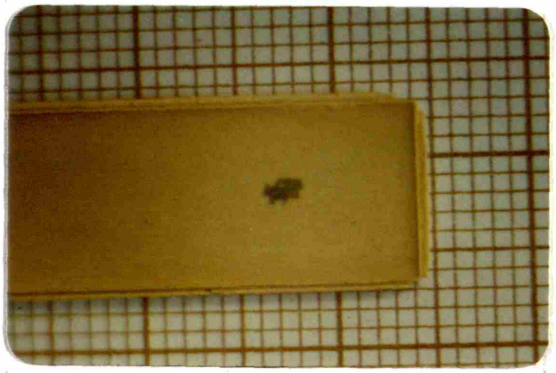

Fig. 6a 2.5X
Tungsten after oxidation at 700°C. Note "cruciform" of oxide. Dark spot on oxide is ink spot from porosity check.

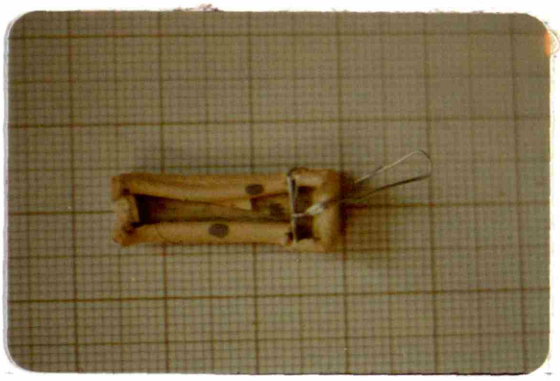

Fig 6b 1.25X
Tungsten after very heavy oxidation at 1000°C. Note that platinum supporting wire is outside of the oxide. Note preferred oxide growth at specimen edges.

FIGURE 6 Photographs of Oxidized Tungsten

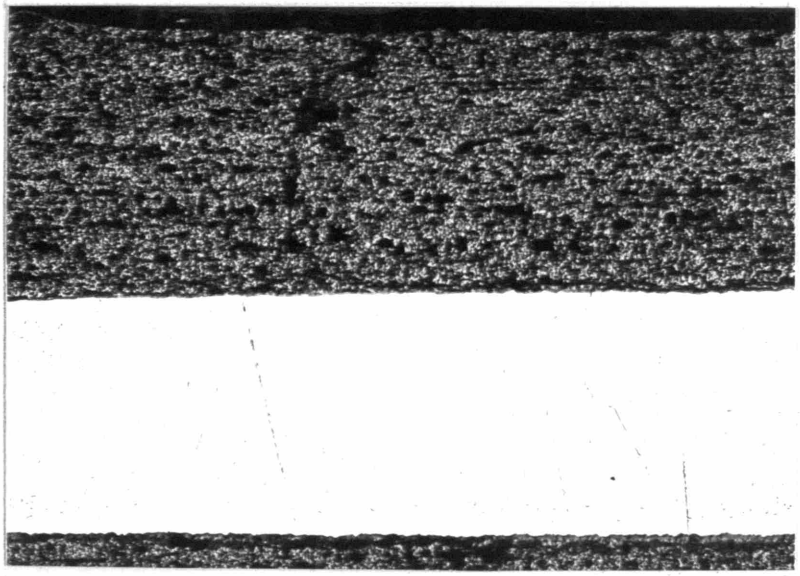

Fig. 7a No etch 100X
Tungsten oxidized at 700°C showing porosity in yellow oxide. Metal is the light area.

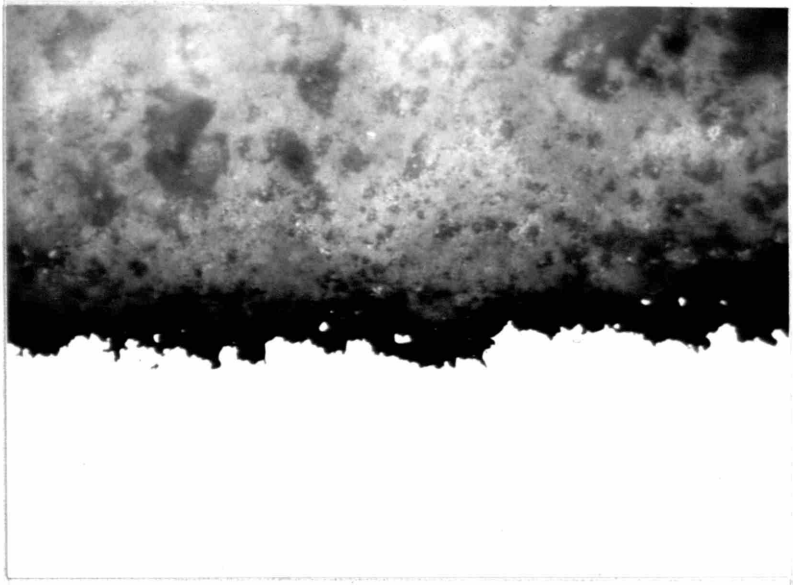

Fig. 7b No etch 2000X
Tungsten oxidized at 700°C observed with oil immersion objective. Dark irregular band in middle is "blue oxide" layer between yellow WO_3 at top and metal at bottom.

FIGURE 7 Photomicrographs of Oxidized Tungsten

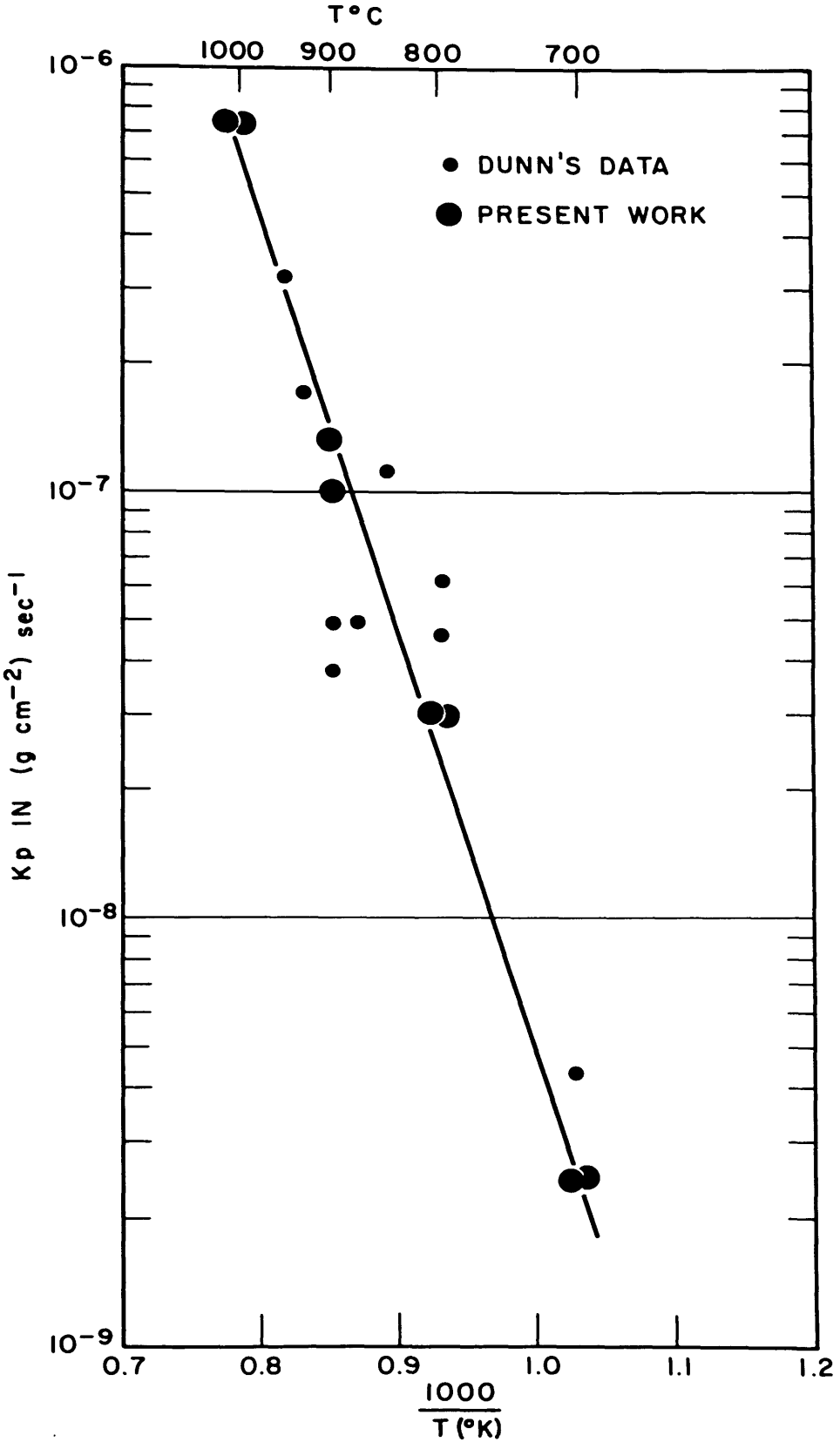

FIG. 8 - ARRHENIUS PLOT OF LIMITING PARABOLIC RATE CONSTANTS FOR THE OXIDATION OF TUNGSTEN

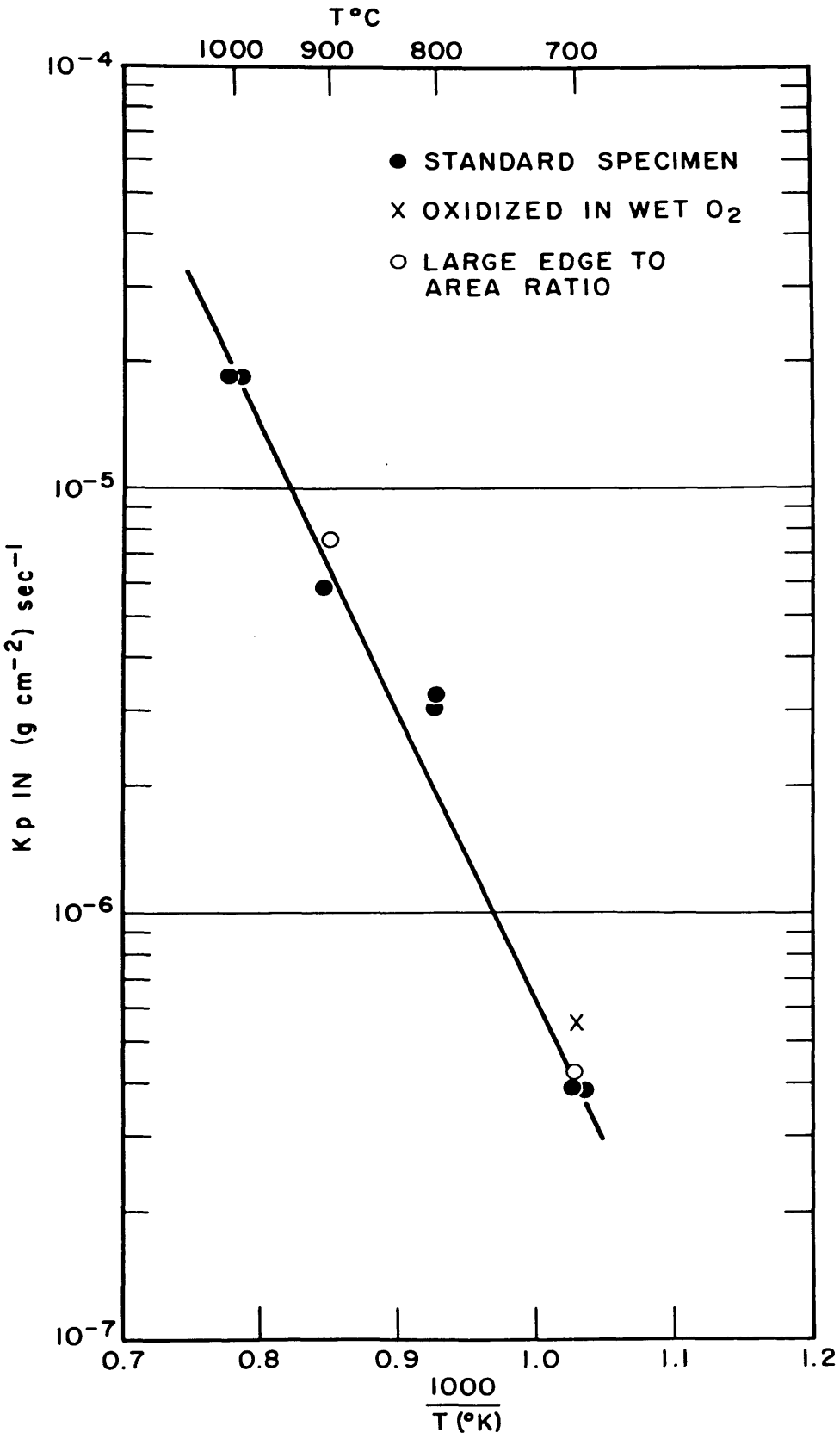

FIG. 9 - ARRHENIUS PLOT OF LINEAR LIMITING RATE CONSTANTS FOR THE OXIDATION OF TUNGSTEN

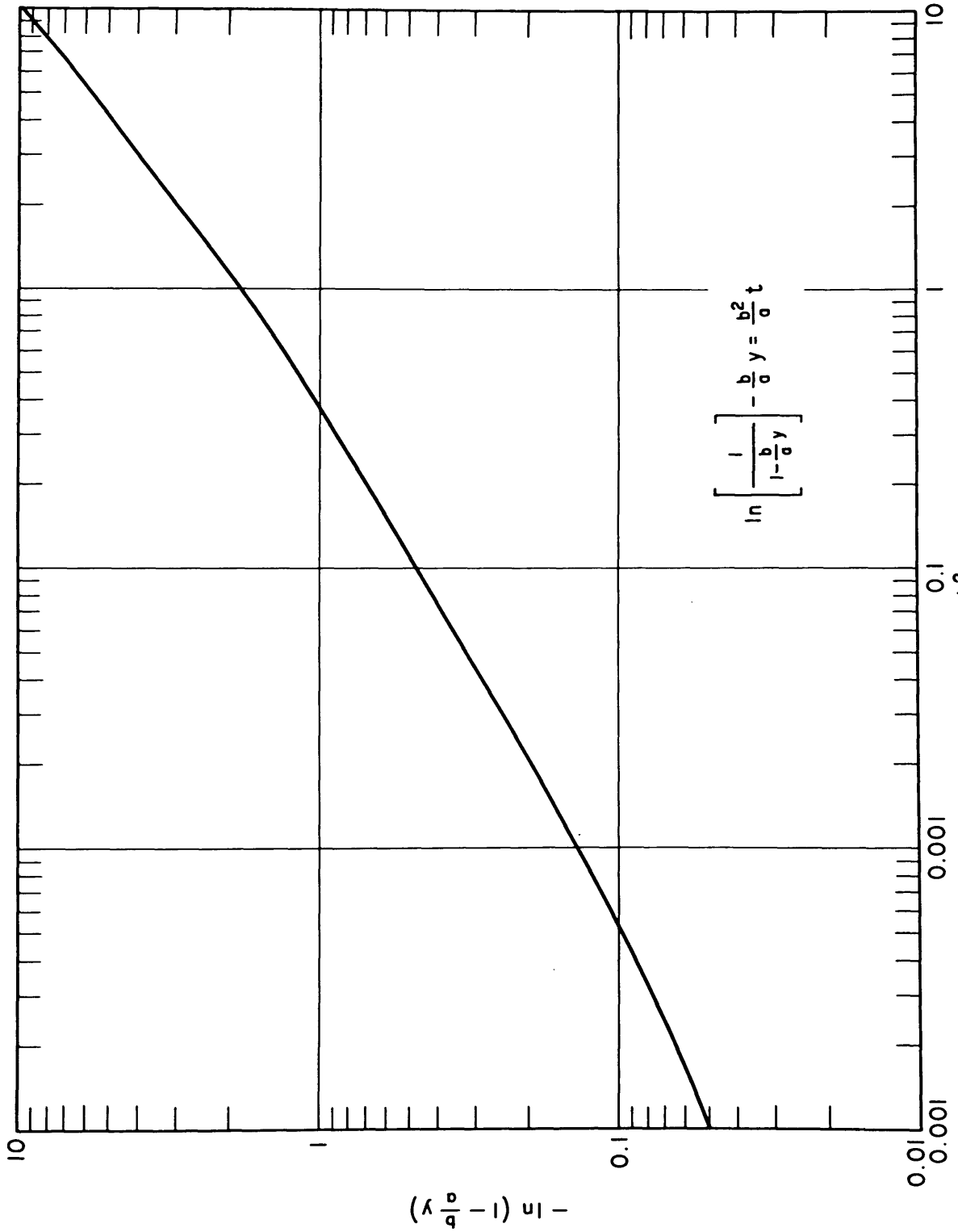

FIG. 10 - EXPRESSION OF THE EQUATION $\frac{b}{a}y + \ln\left(1-\frac{b}{a}y\right) = -\frac{b^2}{a}t$

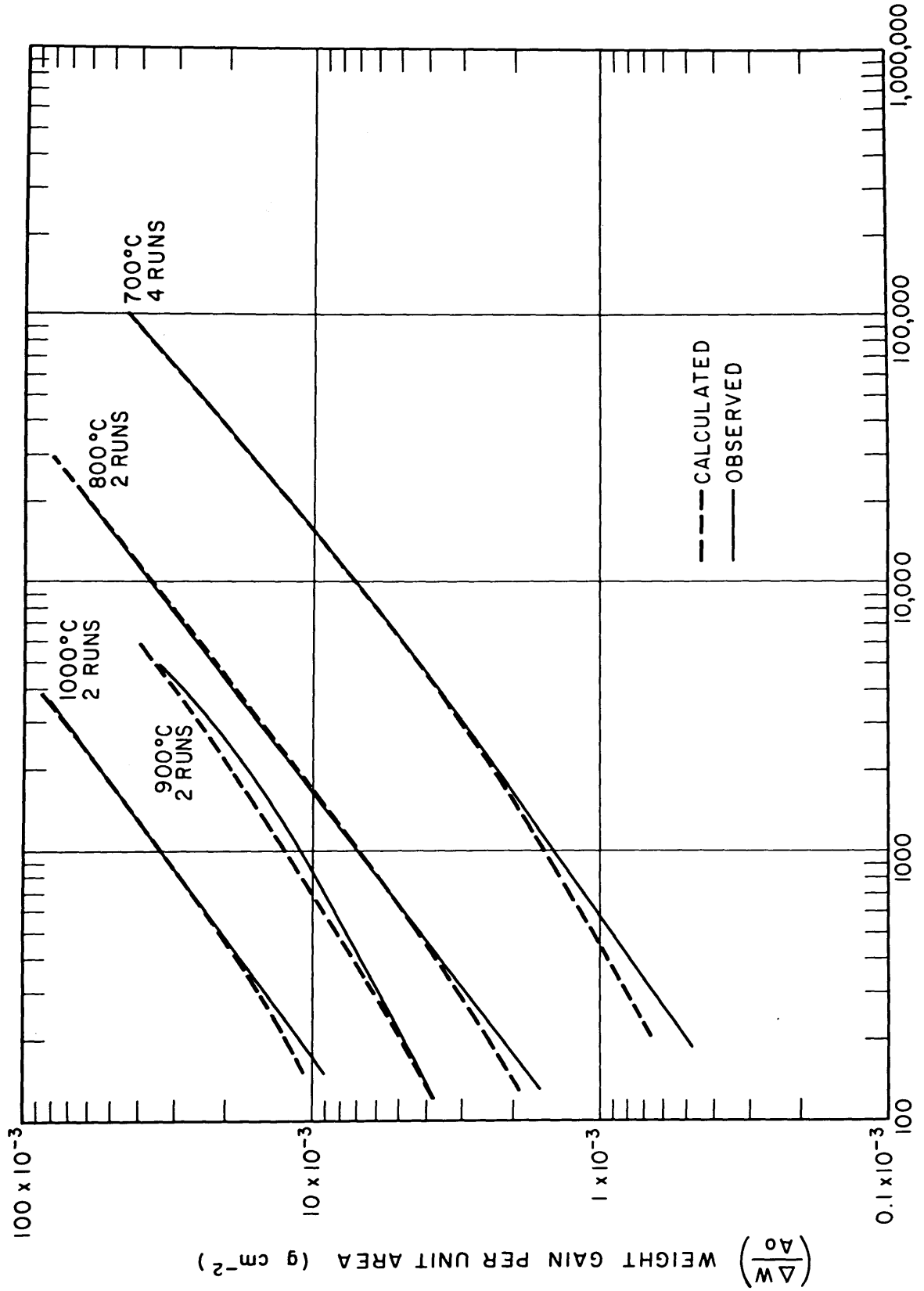

FIG. 11 - COMPARISON OF THEORY WITH DATA ON THE OXIDATION OF TUNGSTEN

IV. OXIDATION THEORY FOR METAL-CARBON SYSTEMS

During oxidation reactions involving metal-carbon systems there is the possibility that one of the reaction products will be gaseous. This possibility is not usually involved in the oxidation of pure metals, however it is essential to the present problem, and this analysis begins with a consideration of where the carbon oxides may form.

A. Theoretical Analysis

In order to fix ideas we may write down a set of generalized simultaneous equations which may represent the reactions involved in oxidation of a metal-carbon alloy

$$M + y/2\ O_2 = MO_y \qquad (1)$$

$$C + 1/2\ O_2 = CO \qquad (2)$$

$$C + O_2 = CO_2 \qquad (3)$$

The possibility that the carbon oxides form at the alloy-oxide interface can then be explored.

Let us make the heuristic assumption that the rate of equation (1) is limited by diffusion through a protective layer of the oxide MO_y, and then test this assumption by calculating from its consequences the behavior of carbon in alloys of the metal-carbon system in certain limiting cases. Specifically let us calculate the total equilibrium pressure of the gases, carbon dioxide and carbon monoxide, at the interface between the metal-carbon alloy and the hypothetical

protective metal oxide. If this pressure is less than atmospheric then there should be no tendency for gas evolution to cause destruction of the protective oxide. On the other hand, if the total pressure of carbon oxides at the alloy-oxide interface is greater than about one atmosphere then pressure would build up mechanical forces around any minute pore which would tend to crack the oxide thus destroying the continuity on which its protective qualities depend.

We may calculate the pressures as follows. To formulate the problem simply, equations (1), (2) and (3) are combined to obtain the virtual reaction

$$CO + 1/y\ MO_y = CO_2 + 1/y\ M \qquad (4)$$

with the corresponding equilibrium constant

$$K' = \frac{P_{CO_2}}{P_{CO}} \ (a_M)^{1/y} \qquad (5)$$

The C - CO_2 equilibrium may be written

$$C + CO_2 = 2\ CO \qquad (6)$$

$$K'' = \frac{(P_{CO})^2}{(P_{CO_2})a_C} \qquad (7)$$

Combining equations (5) and (7) yields expressions for the pressure of the carbon oxides:

$$P_{CO} = K'\ K''\ \frac{a_C}{(a_M)^{1/y}} \qquad (8)$$

and

$$P_{CO_2} = (K')^2 K'' \frac{a_c}{(a_M)^{2/y}} \qquad (9)$$

which may be added to yield the total pressure.

$$P_{CO} + P_{CO_2} = K' K'' \frac{a_c}{(a_M)^{1/y}} \left\{ 1 + \frac{K'}{(a_M)^{1/y}} \right\} \qquad (10)$$

To apply equation (10) the values of K' and K'' may be determined from the available thermodynamic data and an approximation for the minimum value of a_M may be calculated from the properties of the metal-carbon system. If the metal-carbon system contains no stable carbide then either a solution of carbon in the metal or a two-phase mixture of the terminal solution of carbon in the metal plus graphite will be involved so that $a_M = 1$. On the other hand, if a stable carbide is involved, the equations

$$M_xC = C + xM \qquad (11)$$

$$(a_C)\ (a_M)^x = K''' \qquad (12)$$

apply and the activity of the metal may be written

$$a_M = \left[\frac{K'''}{a_C}\right] 1/x$$

where $$K''' = \exp \frac{+\Delta F^o_{MxC}}{RT} \qquad (13)$$

if $F^o_{M_xC}$ is the free energy of formation of the carbide.

In this case equation (10) becomes

$$P_{CO} + P_{CO_2} = \frac{K' K''}{(K''')^{\frac{1}{xy}}} \left[a_C\right]^{(1 + \frac{1}{xy})} \left\{1 + K' \left[\frac{a_C}{K'''}\right]^{\frac{1}{xy}}\right\} \quad (14)$$

Thus the gas pressure of carbon oxides at the alloy-oxide interface may be calculated in terms of the activity of carbon where the activity of graphite at the reaction temperature is taken to be unity. Application of equations (10) and (14) to specific systems is carried out in a subsequent section.

On the basis of this formulation it is now possible to discuss in more detail the limiting classes of behavior of metal-carbon alloys during oxidation.

Class I: $P_{CO} + P_{CO_2} \gg 1$

If on taking reasonable values of a_C, $P_{CO} + P_{CO_2}$ turns out to be substantially greater than one atmosphere, then gas must be evolved with consequent rupture of the metal oxide which had been assumed protective. Thus it is clear that the original assumption fails and in this case it is not possible for a protective oxide to be maintained. There is, however, the possibility that the oxide may heal itself by formation of new oxide in the cracks and pores so that the net result is only a small increase in the oxidation rate.

From the form of equations (10) and (14) this result is to be expected of the more noble metals, that is, those forming the least stable oxides for which the values of K' will be larger.

Comparison of the oxidation behavior of alloys in metal-carbon systems of this class with the oxidation kinetics of the pure metal component of the corresponding system should indicate distinct differences only if the rate of oxidation of the pure metal is limited by diffusion through a protective oxide layer. In this case the rate of oxidation of the carbon-bearing alloy is likely to be distinctly greater than that of the pure metal, and carbon should escape from the sample as a gaseous oxide with consequent degradation of the oxide layer. Consideration of diffusion processes within the metallic portion of oxidizing material yields further detail about the relative rates of formation of metal oxide and carbon oxides.

If it is assumed that diffusion processes within the metal-carbon alloy are negligible, then carbon and metal must oxidize at rates stoichiometrically proportional to their fraction of the alloy composition. Thus, the overall oxidation reaction of a metal carbide might be written:

$$MC_x + (x + y/2)\ O_2 = MO_y + x\ CO_2 \qquad (15)$$

Here x moles of CO_2 are formed per mole of MO_y and the rates of formation of metal oxide and carbon dioxide are strictly proportional.

If on the other hand, diffusion of carbon in the alloy is rapid it is possible that the molar rate of formation of CO_2 is greater than the corresponding molar rate of formation

of metal oxide and the average carbon content of the alloy may decrease during oxidation; that is, decarburization may occur. In this case the rate of formation of CO_2 would be governed by the rate of outward diffusion of carbon from the interior of the test piece. This rate would not be constant so that the linear oxidation law should not apply but the rate of formation of the metal oxide should be high until all of the carbon has been oxidized. After complete decarburization it may happen that formation of additional metal oxide occurring in the pores and crack of the prior metal oxide may result in a complete healing process. If this occurs the rate of formation of further metal oxide will be relatively small since the effective thickness of the oxide layer should be quite large. If healing does not occur, formation of metal oxide may continue at a high rate.

Class II: $P_{CO} + P_{CO_2} \ll 1$ for $a_C = 1$

If solution of equations (10) or (14) yields a total pressure of carbon oxides very much less than one atmosphere then there is the possibility that the carbon may not oxidize at the metal-oxide interface to be evolved immediately as carbon oxides. With this possibility established, alternative behavior must be considered in greater detail to decide whether the metal oxide can really exist as a protective oxide layeer. As the metal is oxidized the corresponding amount of carbon

must be accounted for and three possibilities appear, namely:

Case a. Carbon may dissolve in the metal oxide and diffuse outward through it to form carbon oxides at or near the outer surface of the metal oxide.

Case b. Carbon may be retained in the metal-carbon alloy and diffuse inward in it.

Case c. Elemental carbon or graphite may form at the metal-oxide interface.

These three alternatives are considered individually.

Case a: Solution of carbon in metal oxides has not been studied extensively, but cases are known where complete miscability between an oxide and a carbide occurs. An example is the system TiC - TiO. However, if we consider oxidation of metal-carbon alloys in air or in oxygen at normal pressures the possibility arises that in the interior of the oxide the partial pressure of carbon oxides may be excessive. This is seen by considering the reaction

$$C + O = CO \qquad (15)$$

and the corresponding equilibrium relation

$$P_{CO} = K\, a_C\, a_O \qquad (16)$$

which show that the pressure of carbon monoxide depends on the product of the activities of oxygen and of carbon in the oxide.

For present purposes it may be assumed that solid state diffusion of carbon through the oxide can occur only if the

equilibrium pressure of the carbon oxides never exceeds about one atmosphere. We may explore the condition under which this requirement is met by considering the pressure of carbon monoxide according to equation (16).

With the expected diffusion processes taking place the activities of oxygen and carbon must have their maxima and minima at opposite surfaces of the oxide. In particular, the activity of carbon must be highest at the alloy-oxide interface and lowest at the outer oxide surface; and in contrast, the maximum oxygen activity must be at the outer oxide surface and the minimum at the alloy-oxide interface. Even without assuming any particular form for the activity gradients, the above conditions require that the maximum activity product, and consequently the maximum equilibrium pressure of carbon oxides, must occur somewhere within the oxide.

For the resultant activity product to be small enough that the consequent carbon monoxide pressure is less than one atmosphere everywhere within the oxide, it is necessary that the carbon activity be very low. This is possible only if the diffusion coefficient of carbon in the oxide is large enough that only a relatively small activity gradient is required to obtain a diffusion rate of carbon equal to the rate at which carbon becomes available at the alloy-oxide interface. This becomes clearer if we write Fick's first law for the diffusion of carbon as a quasi-steady state process:

$$J = - D \frac{\Delta C}{\Delta X} \qquad (17)$$

Assuming a linear concentration gradient, oxide thickness ΔX, a carbon concentration near zero at the outer surface, and a diffusion rate j, determined by the rate of oxidation of the alloy, the maximum carbon concentration in the oxide at the alloy-oxide interface is

$$C_{max} = \frac{j}{D} \Delta X \qquad (18)$$

Then of course the carbon concentration and consequently its activity within the oxide must be everywhere less than the maximum calculated above but still the same order of magnitude except near the outer surface.

Since no data is available on such systems only qualitative arguments can be presented. However, in general, the result is that not only must the virtual maximum rate of carbon diffusion through the oxide be great enough to dispose of all carbon made available at the alloy-oxide interface, but the diffusion coefficient must be large enough that the carbon concentration in the oxide is everywhere far enough below saturation to maintain low carbon activities and consequently avoid excessive carbon oxide pressures.

An incidental characteristic of the case where carbon diffuses outward through the oxide is that complete healing of a crack or pore which penetrates part way through the oxide may be prevented since carbon oxides should tend to be evolved at a defect and prevent the reformation of the protective metal oxide there. This may lead to a certain lack

of stability or reproducibility of oxidation rates.

Case b: Inward diffusion of carbon from the alloy-oxide interface into the metallic portion of the test sample may occur under certain conditions. The cardinal necessary condition that must be fulfilled is that the alloy not be saturated with respect to graphite. For if the alloy is saturated with respect to graphite there is no way to establish an activity gradient to act as a driving force for inward diffusion. At the other extreme, if the alloy consists of a non-saturated solid solution, inward diffusion of carbon may occur without formation of an additional phase. This process may be pictured as follows. As metal is removed from the surface of the alloy by oxidation the carbon content at the surface increases above that at the center of the specimen so that a concentration gradient exists in the solid solution. Thus, a driving force for diffusion is created and carbon may diffuse inward. Eventually, in principle, enough metal may be oxidized that the solubility limit is reached. Hereafter another phase must appear and if there is no metal carbide of higher carbon content then graphite is the only possibility. However, if there is an intermediate phase of higher carbon content, such as a metal carbide, this may appear at the surface of the alloy before the interior of the solid solution is saturated with respect to it if the diffusion rate in the initial solid solution is relatively

low. In this case diffusion processes then occur simultaneously in two conjugated layers within the alloy.

The diffusion processes discussed in the above paragraphs may be treated quantitatively by standard methods. The methods for diffusion problems in conjugated layers are rather more complicated but fortunately they have been presented by Jost[23] following an analysis by Professor C. Wagner.

As was noted in Case a, the diffusion of carbon away from the alloy-oxide interface cannot be the rate limiting step in the oxidation process. However, there is no reason why, in principle, both outward and inward diffusion of carbon from the alloy-oxide interface could not occur simultaneously. It should be mentioned further that the exact analysis of the inward diffusion of carbon in the alloy may in some cases be further complicated by solution of oxygen in the alloy during the oxidation reaction because this may have an important effect on the activity coefficient of carbon in the ternary solutions so formed.

Case c: Graphite or free carbon may form at the alloy-oxide interface if diffusion into the alloy and out through the oxide are not adequate to dispose of the carbon freed by oxidation of metal at the alloy-oxide interface. Although the consequences of the formation of graphite are not possible to predict with certainty, there are two obvious possibilities.

It is possible that mechanical degradation of the metal-oxide layer may occur because of stresses developed by the

formation of graphite with its large atomic volume or because of formation of a diffusion barrier which disturbs equilibrium between metal and oxide. On the other hand, if the amount of carbon in the alloy is fairly small the graphite formed may be insufficient to form a continuous layer under certain circumstances. This may be understood by thinking of the graphite which appears at the alloy-oxide interface as an inert marker as is used in a Kirkendall experiment whence it may be seen that if inward diffusion of oxygen is much faster than outward diffusion of metal in the metal oxide layer, then the carbon becomes distributed throughout the oxide simply by movement of the alloy-oxide interface with respect to the graphite previously formed. If on the contrary the outward diffusion of metal is much greater than the inward diffusion of oxygen the graphite accumulates near the alloy-oxide interface.

For one possible set of circumstances the effect of graphite formation (according to the original basis of calculation) is predictable. For alloys in which the calculated pressure of $CO + CO_2$ is less than one atmosphere only because the activity of carbon is quite small in the alloy, then accumulation of carbon till its activity is raised to unity must lead to large carbon oxide pressures. In this case the protective oxide may break down and the behavior becomes like that of Class I.

Summary

The discussion above is probably not exhaustive but it covers those simple limiting cases which appear most likely to be observed in real metal-carbon systems. The results of this semi-quantitative discussion are summarized in Table III, following:

TABLE III

Theory of

Oxidation Kinetics of Metal-Carbon Systems

Class I* Low metal oxide stability: $P_{CO} + P_{CO_2} > 1$

1. Porous metal oxide layer
2. Carbon oxide evolution stoichiometric or preferential
3. Rate greater than for pure metal

Class II High metal oxide stability: $P_{CO} + P_{CO_2} < 1$

a. Outward diffusion of carbon through metal oxide
   1. Protective metal oxide
   2. Stoichiometric evolution of carbon oxides
   3. Rate nearly same as for pure metal
b. Inward diffusion of carbon into alloy
   1. Protective metal oxide layer
   2. Little or no evolution of carbon oxides
   3. Rate nearly same as for pure metal
c. Formation of graphite
   1. Behavior uncertain

* If a protective oxide does not ordinarily form on the pure metal then regardless of the calculated P_{CO} P_{CO_2} the system behaves like those in Class I.

B. Calculation of Carbon Oxide Pressures

Using equation (10) or (14) derived in the preceeding section, the maximum total pressure of carbon oxides at the metal-oxide interface may be calculated in terms of the activity of carbon and metal. However, to obtain absolute pressures, assumptions must be made about these activities. This problem is discussed here with respect to the particular systems for which experiments were carried out. The pressures of the carbon oxides so obtained form a basis for predicting oxidation behavior from the preceeding theoretical analysis.

Tungsten Monocarbide at 700°C and 1000°C: Using equation (14) and assuming $a_C = 1$, it is possible to calculate the carbon-oxide pressures for the equilibrium with WO_2, W_4O_{11} or WO_3 from the equilibrium data available (see Appendix III). However, there is considerable uncertainty in the free energy data for WC and it is also uncertain which oxide to choose. At 700°C for the choice of WO_2 $P_{CO} + P_{CO_2} = 0.1$ atmosphere and for W_4O_{11} $P_{CO} + P_{CO_2} = 7.8$ atmospheres. For W_4O_{11} or WO_3 at 700°C and for WO_2, W_4O_{11} and WO_3 at 1000°C $P_{CO} + P_{CO_2} > 10$ atmospheres.

Nickel plus 2 per cent Carbon at 1000°C: The nickel-carbon phase diagram is a simple eutectic between graphite and nickel with a small fraction of a per cent dissolved carbon. Thus, this composition falls in a two-phase region,

and it is reasonable to take $a_M = a_C = 1$. Applying equation (10), $P_{CO} + P_{CO_2} = 10^6$ atmospheres.

Manganese plus 1.5 per cent Carbon at 1000°C: This composition appears in the gamma terminal solid solution which is, at the solubility limit, in equilibrium with a carbide (usually taken to be Mn_3C). For this composition $a_M = 1$ but it is difficult to guess a good value for a_C. If we take $a_C = 1$ as the upper limit a calculation from available data[7] using equation (10) yields $P_{CO} + P_{CO_2} = 3 \times 10^{-3}$ atmospheres for the equilibrium with MnO. It is possible that carbon may accumulate at the alloy-carbide interface with formation of the metal carbide, Mn_3C. Since a carbon activity gradient must exist in the carbide to permit diffusion we again take the upper limit of $a_C = 1$ and use equation (14) with Kelley's data[25] for the free energy of formation of the metal carbide. This procedure yields $P_{CO} + P_{CO_2} = 0.1$ atmospheres.

Thus, in any case, the maximum pressure of carbon oxides is less than one atmosphere.

Titanium Carbide at 1000°C: There is a wide solubility range for titanium carbide so for an exact calculation one would consider the variation of the activity of metal and carbon in the homogeneous range. However, to compute the maximum pressure of the carbon oxides we may use equation (14) again and take $a_C = 1$. The result of this calculation is $P_{CO} + P_{CO_2} = 0.1$ atmospheres.

V. EXPERIMENTAL STUDIES OF METAL-CARBON SYSTEMS

A. Method of Data Presentation

Each of the following five subsections is essentially autonomous and detailed results are presented independently for each metal-carbon system. Comparison may be made between the experimental results presented here and the theoretical analysis of the preceeding section.

To avoid repetition in each subsection, a brief discussion of the method of data presentation and analysis is given here.

With respect to a generalized reaction of the form

$$(1 - x)\ M + x\ C + \left[\frac{(1 - x)y}{2} + x\right] O_2 = (1 - x)\ MO_y + x\ CO_2$$

we may consider what is gained by experimental measurements of (1) the weight gain of the sample on which the metal oxide forms and (2) the weight of carbon dioxide collected at the exit from the furnace. If both metal and carbon are oxidized, the measured weight gain of the sample and the weight of carbon dioxide collected do not yield directly the amounts of metal oxide formed nor the amount of carbon oxidized. The measured specimen weight gain is accounted for by two factors; namely, (1) the oxygen pick-up due to formation of the metal oxide, and (2) the weight loss due to escape of carbon from the sample. Furthermore, the weight of carbon dioxide collected is of course not equal to the weight of carbon leaving the specimen

since two atoms of oxygen are collected with each atom of carbon. Therefore, correcting factors must be applied to the measured data to "rationalize" them and put them in a useful form.

Oxidation data for pure metals are usually given in terms of the weight increase per unit sample area due to oxygen pick-up by formation of the metal oxide. It is advantageous to present data on metal-carbon systems so that they may be directly compared with results for pure metals so the weight gain data for a metal-carbon alloy must be corrected for the weight loss due to escape of carbon. Furthermore, it is of interest to determine whether carbon or metal is preferentially oxidized from an alloy or whether the oxidation of carbon and metal is strictly proportional to the amounts present in the alloy. Using the known compositions of the alloy and the metal oxide formed, rationalization factors may be derived by which the measured specimen weight gain and the weight of carbon dioxide collected are to be multiplied so that (1) plots of these corrected values on the same scale will virtually coincide if the oxidation is non-preferential and (2) these plots may be directly compared with a weight gain plot for a pure metal. In terms of the generalized reaction presented above the rationalization factors are:

$$\frac{\text{Weight gain}}{\text{sample area}} = \frac{16\,y\,(1-x)}{16\,y\,(1-x) - 12x}$$

$$\frac{\text{Carbon dioxide collected}}{\text{sample area}} \cdot \frac{12}{14} \cdot \frac{16\ y\ (1 - x)}{12x} = \frac{16}{44} \frac{y(1 - x)}{x}$$

(Weights in grams; areas in square centimeters.)

We take for an example the oxidation of titanium carbide according to the reaction.

$$TiC + 2O_2 = TiO_2 + CO_2$$

Here $y = 2$ and $x = 0.5$ so the rationalization factors are:

$$\frac{\text{Weight gain}}{\text{sample area}} \cdot \frac{32}{20}$$

$$\frac{\text{Carbon dioxide collected}}{\text{sample area}} \cdot \frac{32}{44}$$

If the rates of oxidation of titanium and carbon are strictly proportional to the amounts present in TiC, that is, if one mole of carbon is oxidized for every mole of titanium, a plot versus time weight change and weight of carbon dioxide collected, multiplied by these factors, should yield just one curve. The numerical values on the ordinate of this plot indicate directly the amount of oxygen pick-up due to formation of TiO_2 and may be compared directly with the values for pure titanium.

B. Tungsten Carbide

Introduction: Only comparative measurements of the oxidation of the tungsten carbides are available but considerable comparative data is available on the oxidation of various commercial hard metals containing tungsten carbides. Some of this work is discussed in recent thesis research carried out at M.I.T.[5] Tungsten monocarbide, a widely used primary constituent of commercial hard metals, is known to have poor oxidation resistance following the linear rate law[26].

Calculation of the pressures of the carbon oxides in equilibrium with tungsten monocarbide and either "W_4O_{11}" or WO_3 yields pressures above one atmosphere with a_C taken as 1 so it is to be expected that gas would be evolved during oxidation with consequent distruction of the protective oxide that might otherwise form. In the preceeding section the oxidation of tungsten was discussed and the results for tungsten monocarbide presented here are compared with those results.

Preparation of Tungsten Carbide: Three methods were tried for preparation of suitable tungsten carbide samples. Cold pressing and subsequent sintering at 1700°C resulted in porous briquettes subject to internal oxidation and disintegration during oxidation. However, suitable specimens were prepared by hot pressing pure tungsten carbide powder. The resulting material had relative density of about 90 per

cent. The third method, although proving unsatisfactory as a source of specimens for the present research, produced an interesting anamoly. Tungsten carbide was made by diffusing carbon into solid tungsten sheet. This was accomplished by packing the tungsten sheet in ground spectroscopic carbon (National Carbon Co., Cleveland, Ohio) and heating at 1450°C for about 24 hours in a stream of dry hydrogen at 1 atmosphere pressure or at 1700°C for 1 hour in argon. The resultant specimens had tungsten carbide cases of the order of 50 microns thick. The carbides were identified by X-ray diffraction. No W_2C was observed in X-ray diffraction patterns taken directly on the outer surface of the samples or in patterns of a sample with a thin carbide layer after crushing it to powder, nor was a W_2C layer identified by microscopic study. However, after grinding, oxidizing, or dissolving away the outer-most layer the diffraction pattern of W_2C appeared. The conditions selected for diffusion were based on the results of Pirani and Sander[42] who have determined a diffusion coefficient, D_c, which they suggest applies to interdiffusion in WC. Their experiment involved measuring the rate of growth of the carbide layers on solid tungsten heated in carbon. The thickness of the carbide layers formed in the present work agrees with that expected from their data. However, they found no W_2C as would be expected if they had examined only the outer carbide layer. It might be pointed

out that in the well known work of Sykes[49] on the tungsten carbon system, W_2C was found in diffusion specimens between the W and WC layers.

Results: The oxidation rate data obtained for tungsten monocarbide are presented in Figure 12 with typical data on tungsten for comparison. Photographs of oxidized specimens appear in Figure 13. The results at 1000°C are of qualitative value only because the rate exceeded that which could be accurately measured with the equipment available. However, at 700°C the rate observed is constant, that is, the linear rate law applies. The amount of carbon dioxide formed corresponds to that expected according to the reaction

$$WC + \tfrac{5}{2}O_2 = WO_3 + CO_2$$

The data are stoichiometrically rationalized and plotted so that the weight of oxygen retained in the scale (as WO_3) per square centimeter second is just the slope of the plot. Rationalization involved multiplying the measured amount of carbon dioxide by the ratio 48/44 and the measured weight gain by the ratio 48/36. This mode of plotting makes possible direct comparison with the weight gain data for pure tungsten. The linear rate constant on this base observed for tungsten monocarbide at 700°C is 4×10^{-6} g cm^{-2} sec^{-1}. The rate of oxidation of the carbide greatly exceeds that for tungsten at all times.

Only yellow tungstic trioxide was formed and there was no sign of the "blue oxide" under it. Thus it may be concluded

that formation of the protective blue oxide which appears during the oxidation of tungsten was prevented by the evolution of carbon oxides during the oxidation of tungsten monocarbide.

Similar rates were obtained for tungsten carbide sheets formed by diffusion of carbon into solid tungsten which suggests that the comparison of results on tungsten carbide having appreciable porosity with results for porosity free tungsten is valid. The data obtained for tungsten carbide sheets is not reported in detail since the composition of the material was not uniform.

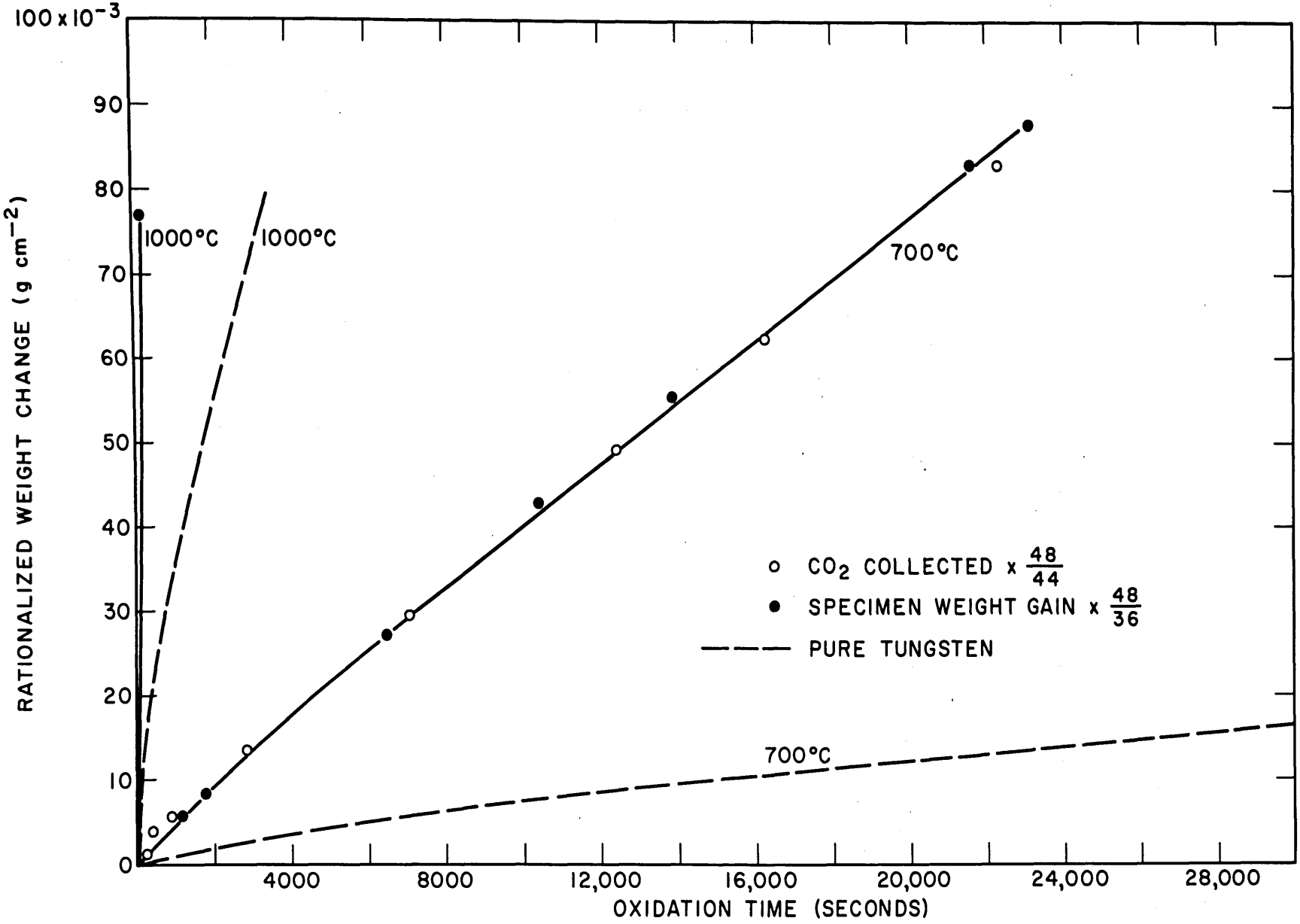

FIG. 12 - RATIONALIZED DATA ON THE OXIDATION OF TUNGSTEN CARBIDE

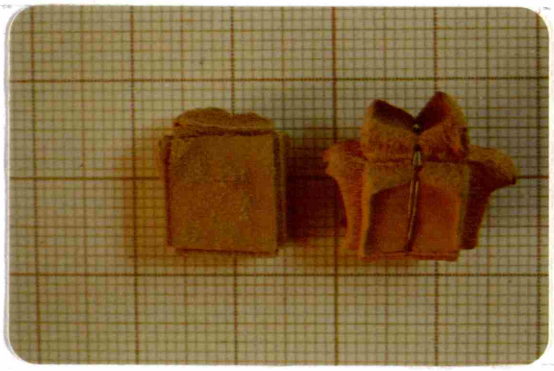

1.25X

Oxidized tungsten carbide. Sample at left oxidized at 700°C and sample at right oxidized only a few minutes at 1000°C.

FIGURE 13 Photograph of Oxidized Tungsten Monocarbide

C. Nickel-Carbon Alloys

Introduction: The nickel-carbon system was selected as a particularly convenient representative of those metal-carbon alloys from which evolution of carbon dioxide during oxidation might be expected to disrupt the protective metal-oxide layer. The conditions under which this might be expected to occur are discussed in Section IV. The oxidation of nickel of various purities has been intensely studied (see index in Kubaschewski and Hopkins[28]) and it is known to follow the parabolic rate law with a relatively small rate constant at high temperatures. Cationic diffusion has been suggested as the principal mechanism of diffusion in nickel monoxide (NiO) which is the only oxide normally formed. The nickel-carbon system is a simple eutectic with no stable carbide and 0.27 per cent carbon soluble in nickel at 1000°C.[30] Thermodynamic calculations using the equation discussed in Section IV B and established data indicate that the equilibrium pressure of carbon dioxide in equilibrium with nickel and nickel oxide is on the order of 10^6 atmospheres. Hence, formation of carbon dioxide should occur at the nickel - nickel-oxide interface during oxidation.

Experimental Procedure: A nickel-carbon alloy analyzing about 2.3 per cent carbon was made by induction melting pure nickel (Vacuum Metals Corp., Cambridge, Mass.) of nominal composition:

Element	Weight Per Cent
C	0.004
O	0.002
N	0.000037
S	0.0045
Co	0.003
Si	0.003
Ni	99.986 (by difference)

and alloying this with chips of spectroscopic carbon (National Carbon Company, Cleveland, Ohio). Melting was carried out in an aluminum oxide crucible under purified argon atmosphere. Specimens were obtained by sucking the liquid alloy into Vycor tubing and allowing it to freeze there. Shiny, smooth surfaces were obtained but these were abraded in the usual manner before oxidizing. The structure of the as-cast alloy is shown in Figure 14a. It is graphite in nodular and flake form in a matrix of nickel-carbon solid solution.

Results: Pure nickel was found to follow a parabolic rate law quite closely and at 1000°C the parabolic rate constant was about 4×10^{-10} (g-cm^{-2})^{2}sec^{-1} in agreement with the results of previous investigations on high purity nickel (see Kubaschewski and Hopkins[28] pages 68 and 69).

Data on the nickel-carbon alloy indicated that carbon oxides form rapidly during the early stages of oxidation so that the samples tested were totally decarburized within about 60,000 seconds (17 hours). While the carbon was being

oxidized, the rate of formation of nickel oxide was also rapid but once all of the carbon had been removed the rate of oxidation became very low, indicating that the nickel-oxide layer had become protective. The data are presented in Figure 15. The weight of oxygen in the nickel oxide formed turns out coincidently to be nearly equal to the weight loss due to removal of carbon so the net changes of sample weight are quite small negative values. The difference between the two recorded runs is almost certainly due to variation of alloy composition amongst test samples. Evolution of carbon dioxide is shown by the uppermost curve. By correcting the sample weight change for the carbon loss, the weight of oxygen in the oxide is derived. This curve represents the amount of scale formation which may be compared with the oxidation curve for pure nickel presented in the same figure.

Discussion: The high rate of evolution of carbon dioxide requires that carbon be removed from the interior of the sample. This is confirmed by the disappearance of graphite shown by Figure 14b, a photomicrograph taken of a sample nearly depleted of carbon. Comparison may be made with the original structure shown in Figure 14a. That outward diffusion of carbon through the metal is the rate limiting step in the formation of carbon dioxide is suggested by agreement between the observed formation of carbon dioxide and calculations presented in Appendix IV. These calculations lead to

a value of about 2×10^{-6} cm^2 sec^{-1} for the diffusion coefficient of carbon in fine-grained polycrystalline nickel at 1000°C in comparison with the published value of 3×10^{-7} cm^2 sec^{-1} for a coarse-grained nickel[30].

Although the rate of formation of nickel oxide must depend on the damage done to the proctive layer on the alloy by gas evolution no detailed mechanism can be suggested. Incidentally, the oxygen pick-up due to formation of nickel oxide (in grams) is close to loss of carbon (in grams). The fact that the rate of nickel oxide scale formation after complete decarburization drops to values lower than those observed after equal times for pure nickel indicate that damage to the oxide caused by gas evolution heals later to permit re-establishment of the protective oxide layer. In Figure 14c the structure of the oxide and metal near the surface are shown at a stage when most of the carbon has been removed. The oxide appears as two layers of nickel monoxide which merge without a sharp boundary. The inner layer is a very porous aggregate of fine grains but the outer layer has a coherent structure pierced by some large pores. It is probable that most of the pores visible in the outer layer were actually formed by inadequate polishing but the porosity of the inner oxide layer below the polished surface was clearly observed by use of dark field and plane polarized illumination. It is probable that the porous part

of the oxide was formed during early stages of the oxidation while gas was being evolved rapidly and that the less porous outer part was formed later when gas evolution was not so rapid. It was unfortunately not possible to obtain for comparison a satisfactory polished section through the oxide on pure nickel due to its lack of adherence at room temperature. It appears however, that healing of pores does occur in the oxide on nickel-carbon alloys after cessation of gas evolution.

Conclusions: During the oxidation of a nickel-carbon alloy carbon oxide gases are evolved with consequent damage to the protective nickel oxide layer. Thus the rate of scale formation is quite high so long as gas is being evolved, but later healing of the nickel oxide occurs and the rate of oxidation becomes very low. Oxidation of carbon from the alloy appears to be limited by diffusion within the alloy.

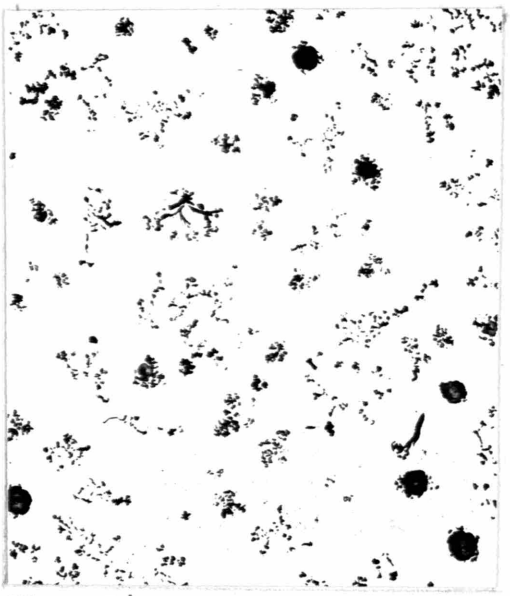

Fig. 14a 100X
Nickel + 2.3% carbon as cast. Graphite in nickel carbon solid solution matrix.

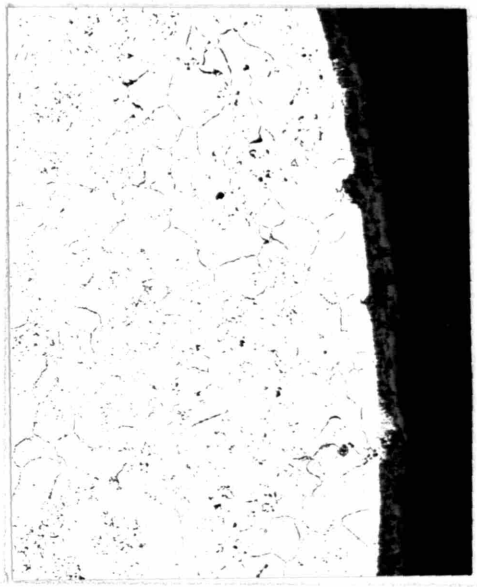

Fig. 14b 100X
Nickel + 2.3% carbon after oxidation has removed most of the carbon. Voids appear in nickel matrix.

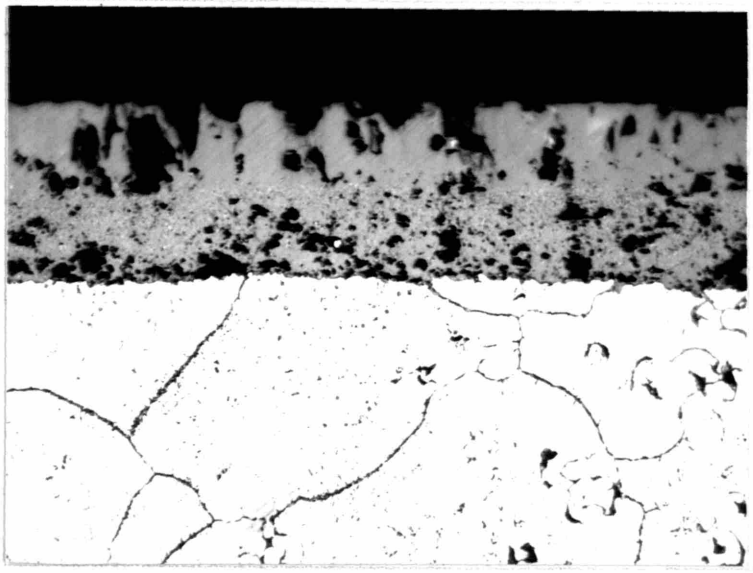

Fig. 14c 500X
Oxide on nickel-carbon alloy after oxidation. Oxidation of graphite phase has left voids in metal. Oxide appears as two layers, inner layer highly porous. Oxide is the grey region near the top of the print. Some intergranular oxidation of the nickel is apparent.

FIGURE 14 Photomicrographs of Nickel-Carbon Alloys
(All etched with HNO_3 HA_c)

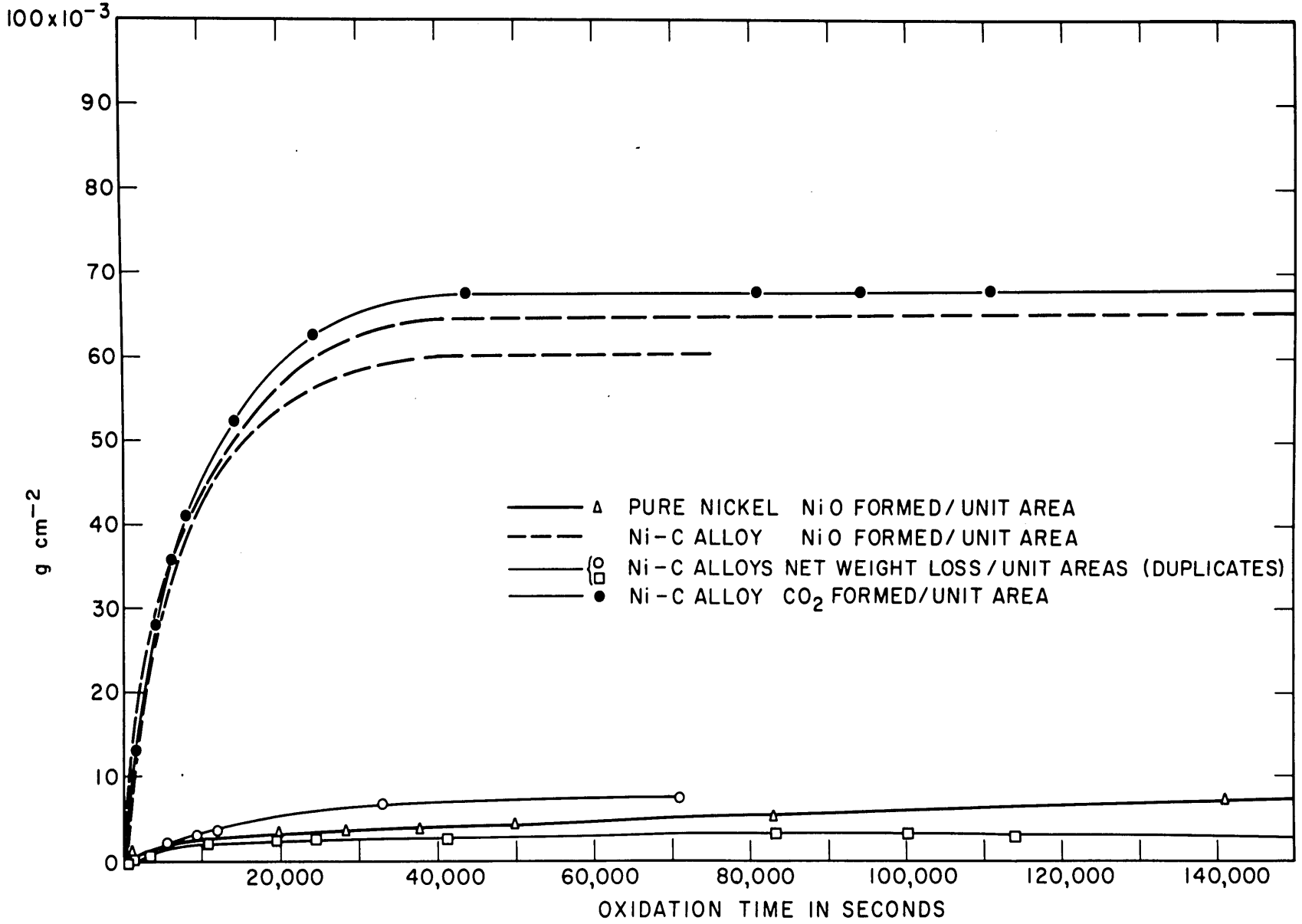

FIG. 15 - OXIDATION OF NICKEL-CARBON ALLOYS AT 1000°C

D. Manganese Carbon Alloys

Introduction: The system manganese carbon was selected as a likely representative of those metal-carbon alloys which might be expected to oxidize without formation of carbon oxides. The conditions under which this might occur are discussed in Chapter IV.

The oxidation of pure manganese has been successfully studied by Gurnick and Baldwin[16] who overcame the tendency of manganese samples to disintegrate on heating by electroplating manganese on a strong base material. They found that the parabolic law was followed during oxidation in air between 400 and 1100°C. The rate constant they measured at 1000°C (the temperature used in the present work) is about 5×10^{-8} $(g\ cm^{-2})^2\ sec^{-1}$. They report that the oxide formed in air at this temperature was about 10 per cent MnO, and 90 per cent Mn_3O_4.

The manganese-carbon phase diagram has been studied by Isobe[20] and by Vogel and During[51] who have shown that there is a high temperature γ' phase, similar to γ' iron, which dissolves carbon up to about two weight per cent at 1000°C. At higher carbon contents there is disagreement about the carbide phases that occur. However, there seems to be a high temperature carbide with a homogeneity range from about three weight per cent to four weight per cent carbon at 1000°C. This carbide transforms in an uncertain

way on cooling. The available information on the manganese carbides has been summarized by Kuo and Persson[29].

Thermodynamic calculations using the methods discussed in Section IV and data reported by Coughlin[7] and by Kelley[25] indicate that the equilibrium pressure of carbon dioxide and carbon monoxide in equilibrium with either Mn_3C or carbon bearing γ manganese and with MnO is substantially less than one atmosphere. Hence, it is possible that the chemical potential of carbon in γ manganese is low enough to permit retention of carbon in the sample as the manganese is oxidized rather than evolution of carbon as a carbon oxide gas.

Experimental Procedure: Samples were made by induction melting electrolytic manganese (Electro Metallurgical Co., New York, N.Y.) of reported analysis

Fe	0.92	weight	per	cent
Si	0.21	"	"	"
C	0.10	"	"	"
Mn	98.6	"	"	"

and alloying this with chips of spectroscopically pure carbon electrodes (National Carbon Co., Cleveland, Ohio). Melting was carried out in an aluminum oxide crucible under a purified argon atmosphere.

Specimens were obtained by sucking the liquid metal into "Vycor" glass tubing. Oxide-free surfaces resulted but

specimens of both manganese and the manganese-carbon alloy invariably cracked during cooling. However, it was possible to select suitable pieces, cut them to size, abrade their surfaces and reheat them for oxidation experiments without disintegration.

X-ray diffraction, metallography and chemical analysis indicated that the "pure" unalloyed manganese test pieces, containing 0.21 weight per cent carbon, consisted of β manganese plus a little α manganese. The manganese-carbon alloy, containing 1.33 weight per cent carbon, consisted chiefly of α manganese with slightly smaller lattice parameters than usually reported and an additional phase, probably of one of the manganese carbides. Figure 16a shows the structure of the alloy after reheating to 1000°C for several hours and air cooling to simulate the heat treatment undergone during oxidation testing. Virtually no observable change of microstructure was incurred by this treatment.

Oxidation of test specimens was carried out using the techniques previously described. The test pieces were examined after oxidation by X-ray diffraction and metallography, and their carbon contents were determined by combustion methods.

Results: Unalloyed manganese was found to oxidize according to the parabolic rate law with rate constant $k_1 = 5 \times 10^{-8}$ (g cm^{-2})^2 sec^{-1} in excellent agreement with the

results of Gurnick and Baldwin[16]. The data are presented in Figure 17.

Oxidation of the manganese-carbon alloy also followed the parabolic rate law except for a small initial deviation which probably is due to oxidation observed in cracks in the specimens used. The rate constant observed is 7×10^{-8} $(g\ cm^{-2})^2 sec^{-1}$ which is only slightly higher than was observed for pure manganese. However, the measured amount of carbon dioxide formed from carbon escaping from the specimen was far below that corresponding to non-preferential oxidation of carbon from the alloy. A stoichiometric calculation indicates that about 0.17 grams of carbon dioxide should be formed per gram weight change of the specimen during oxidation if preferred oxidation of carbon or of manganese does not occur. Using the reciprocal of 0.17 as a rationalizing factor, the measured amount of carbon dioxide may be compared with the specimen weight change. The experimental results plotted on this basis are presented in Figure 17. If all of the carbon in the alloy were oxidized stoichiometrically, the weight gain per unit area and the carbon loss curves would coincide on this plot. However, it is clear that practically none of the carbon has escaped from the specimen. This result was confirmed by a duplicate run during which the total amount of carbon dioxide formed was absorbed in one weighing bottle.

The total amount of carbon dioxide evolved during a run of 44 hours (160,000 seconds) was 0.007 grams (about four times the minimum measurable value) which is less than one-twentiety of that expected if carbon and manganese were oxidized stoichiometrically according to the composition of the alloy. In the course of the 44-hour oxidation run, about one-half of the manganese originally present in the sample was oxidized so that the average carbon content of the metal roughly doubled, reaching about 2.6 per cent.

That nearly all the carbon actually does remain in the manganese during oxidation is clearly confirmed by a carbon analysis of a representative sample of the metal after 25 hours (90,000 seconds) of oxidation. The analysis showed 2.15 weight per cent carbon in agreement with the amount expected assuming that it all remains in the specimen.

Metallographic examination of the metallic portion of the test pieces after oxidation indicated the presence of a distinct layer about 100 microns thick at the surface. An X-ray diffraction pattern of the sample crused to powder revealed α manganese as the primary constituent with a substantial amount of an additional phase which is probably a manganese carbide. The surface layer alone yielded the diffraction pattern of β manganese with an additional phase which may or may not be the same as that in the interior of the sample. Figure 16b shows the microstructure of these layers.

The oxide formed as a solid greenish-black coherent shell around the samples. It consisted chiefly of MnO, but the presence of some Mn_3O_4 was indicated by an X-ray diffraction pattern. Figure 16c is a photomicrograph of the oxide and a portion of the metal cores. The oxide appears to have recrystallized in its outer layers into very large grains. Before etching to bring out the grain boundaries a fine precipitate was observed, primarily in the outer portions of the oxide. It is likely that this is Mn_3O_4 precipitated during cooling. It was observed that there was a substantial gap between the metal cores and the oxide. This gap was loosely filled with a grey metallic-appearing crystalline powder which could not be identified readily.

Discussion: It appears certain that nearly all of the contained carbon is retained in the test pieces during oxidation of manganese containing up to at least 2.6 per cent carbon. Thus, only the very small observed increase in the oxidation rate constant of the manganese-carbon alloy, as compared to unalloyed manganese, is to be expected in this case since very little carbon passes through the oxide layer.

Although no direct data on the diffusion mechanism through the oxide layer was obtained, it is possible to gain some insight by analogy. Considering the isomorphism of MnO and Wustite, and the similarity in the chemistry of iron and manganese oxides, it is likely that the principal mechanism

of diffusion through them is the same. Jette and Foote[22] have shown that cation vacancies are the principal defects in the Wustite lattice and Pfeil[40] has observed gaps between metal and the oxide formed on iron just as were observed in the present case on manganese and the manganese-carbon alloy. Furthermore, Davies, Simnad and Birchenall[9] have shown that cation diffusion dominates in the Wustite layer during the high temperature oxidation of iron. Therefore, it is likely that the observed gap between manganese metal and its oxide, MnO, during oxidation is due to outward diffusion of manganese resulting in mass transfer outward. Since the specimens are cylindrical, the oxide has the form of a pipe which cannot contract inward without plastic flow. It is possible that the powder in the gap acts as a diffusion path for mass transfer across this gap. McDonald and Dravnieks[37] have considered this problem in a general way and have suggested that the type of gap observed here may frequently occur.

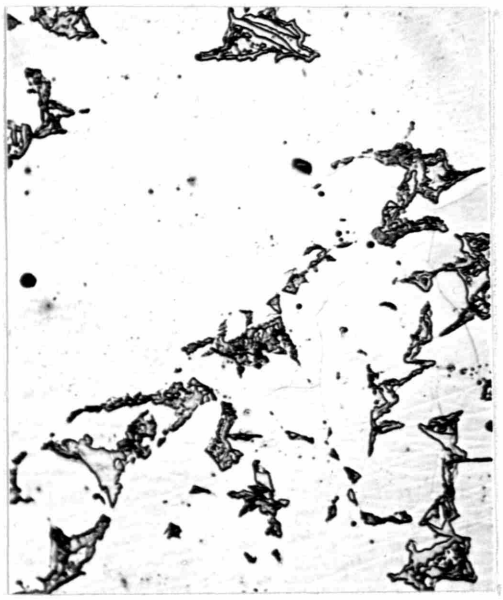

Fig. 16a 500X
Nital etch
Manganese-carbon alloy annealed at 1000°C for 1 hour. Precipitate in ∝ manganese matrix.

Fig. 16b 500X
Nital etch
Manganese-carbon alloy after 90,000 sec. oxidation. Core structure at left is primarily ∝Mn. Outer layer is at right.

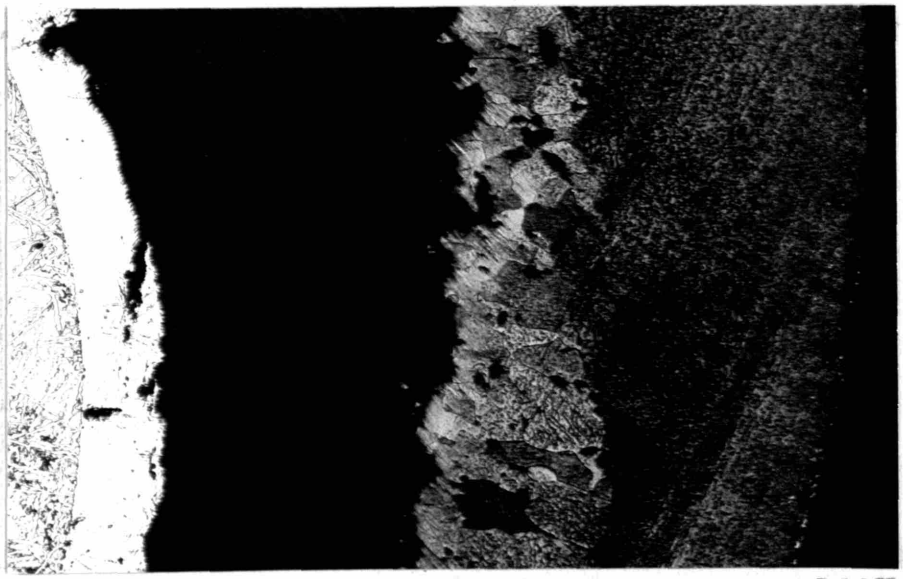

Fig. 16c Light Nital Etch 100X
Manganese-carbon alloy after 90,000 sec. oxidation at 1000°C. From left to right structures are: metallic core with distinct outer layer almost white; dark area of mounting compound; oxide layer of MnO with Mn_3O_4 precipitate.

FIGURE 16 Photomicrographs of Manganese-Carbon Alloys

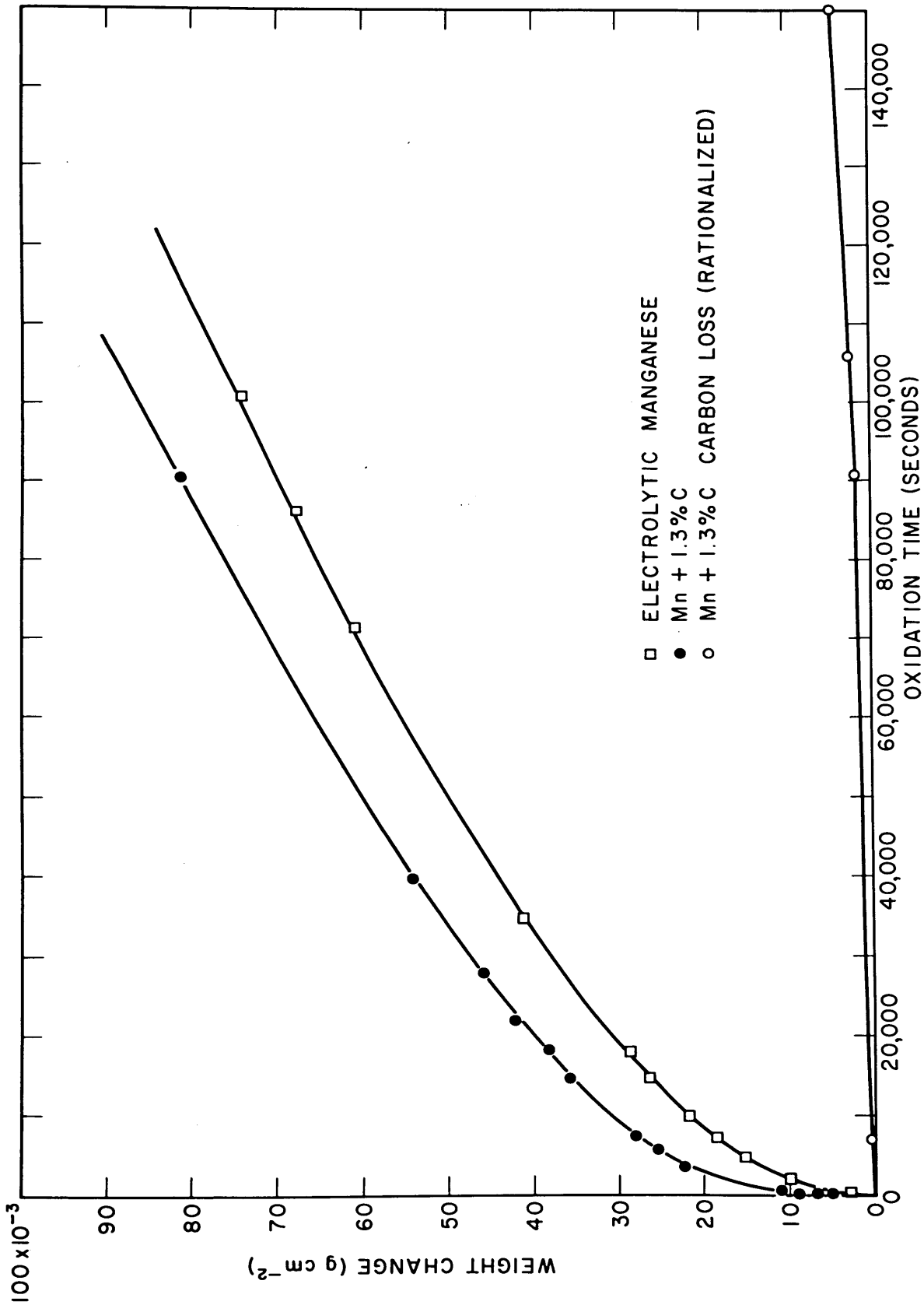

FIG. 17 - OXIDATION OF MANGANESE AND A MANGANESE-CARBON ALLOY

E. Titanium-Carbon System

Introduction: The titanium-carbon system, besides being of commercial importance, was selected as a convenient representative of that group of metal-carbon systems in which the pressure of carbon oxides in equilibrium with the carbide and the highest oxide is small. The titanium-carbon system has a small terminal solid solution and a very stable carbide, TiC, with a substantial homogeneity range[47]. The titanium-oxygen system is characterized by large terminal solid solubility of oxygen in titanium and by at least three oxides; TiO, Ti_2O_3, and TiO_2[6][11]. Although quite a lot of work on the oxidation of hard metals based on TiC has been reported, no published data on TiC has appeared. Some data at 1000°C obtained by H. Blumenthal[2] have not been published. He found that the parabolic rate law applied, that the rate constant is near the value for titanium, and that iron as an impurity increases the oxidation rate. The oxidation of pure TiC has been studied in some detail and the references through 1954 are given by Simnad, Spilners and Katz[48]. The oxidation of pure titanium at high temperatures follows the parabolic rate law fairly well, but it appears that there are two simultaneous processes; namely, solution of oxygen in titanium and formation of a layer of titanium dioxide. Simnad, Spilners and Katz have experimentally separated these processes and given rate constants applying to the formation of the TiO_2 layer alone. Their value at 1000°C is about 10^{-8} g^2 cm^{-4} sec^{-1}.

Preparation of Specimens: Commercially pure titanium carbide powder was hot pressed into specimens having apparent densities in excess of 97 per cent. Titanium metal specimens were cut from swaged rods of vacuum melted iodide titanium. A carbon deficient titanium carbide containing 15.78 weight per cent carbon was made by reacting stoichiometric TiC with titanium powder reported to be 99.9 per cent pure (A. D. McKay Company) at 1600°C in vacuum for 1 hour. The resultant compacts were readily recrushed to provide a powder of carbon deficient titanium carbide corresponding to the formula $TiC_{0.63}$. An X-ray diffraction pattern of this material showed a sharp pattern of TiC (with reduced lattice parameter) which indicated uniform composition. Subsequent hot pressing yielded rather porous specimens which were contaminated by carbon at their outer surfaces. The contamination was removed by grinding, and inspection of specimens after oxidation indicated that following an initial period of a few minutes internal oxidation was probably negligible.

Results: The data on the oxidation kinetics for pure titanium, carbon deficient titanium carbide and stoichiometric TiC are presented in Figure 18. The data supporting each curve drawn were obtained during several duplicate runs in most cases. It was observed that the formation of the metal oxides at 1000°C takes place at about the same rate on titanium metal and on the carbon deficient titanium carbide, and that

stoichiometric titanium carbide reacts at a slightly slower rate. The data plotted in Figure 18 are rationalized so that the ordinate scale represents the equivalent amount of oxygen take-up due to formation of TiO_2 according to the reaction

$$TiC_x + (1 + x)\ O_2 = TiO_2 + xCO_2$$

The rationalization factors are:

$$\frac{\text{Weight gain}}{\text{area}} \text{ multiplied by } \frac{32}{32 - 12x}$$

$$\frac{CO_2 \text{ evolved}}{\text{area}} \text{ multiplied by } \frac{32}{44x}$$

With these rationalization factors, nonpreferential oxidation and evolution of carbon is indicated by the observed superposition of the normalized curves of sample weight gain and gas evolution. Although there was the possibility for inward diffusion of carbon during oxidation of the carbon deficient titanium carbide this evidently did not occur. The rationalized oxidation data for the carbides may be directly compared with the weight gain curves for the pure metal.

From Figure 18 one sees that carbon is stoichiometrically oxidized and that the rate of oxidation of the carbides is not greater than that of pure titanium. The present data on pure titanium yield a higher parabolic rate constant than the data of Simnad, Spilners and Katz[48] on both pure titanium and titanium saturated with oxygen, and if their results are taken for comparison, the oxidation of the titanium carbide,

TiC, seems to proceed at about the same rate as pure titanium. It is difficult to decide whether to compare the results on titanium carbide with the present data on pure titanium or with the results of Simnad, Spilners and Katz. It is possible that the lack of presaturation of the specimens with oxygen has a large effect on the present results, but a comparison with Simnad, Spilners and Katz is not possible since they do not give the thickness and shape of their samples, and the magnitude of the effect of oxygen solution in the metal depends on the volume-to-area ratio. At 900°C the data of Jenkins[21] on the oxidation of commercial titanium are available, but he does not give his results on iodide titanium other than to say that the oxygen pick-up is larger. His data indicate that the rates of oxidation of TiC at 900°C are greater than the rates of oxidation of commercial titanium at 900°C. In view of this uncertainty the possibility that the oxidation of stoichiometric titanium carbide is significantly slower than the oxidation of titanium must be considered. Such an effect could be due to carbon dissolved in the titanium dioxide on the carbide, to other impurities oxidized from the carbide, or even to an entirely different rate limiting mechanism. It is actually possible that the rate limiting step in the oxidation of the carbide is really an interface reaction rather than diffusion especially since a parabolic rate law is not exactly observed

in this case.

Oxidation of the titanium carbides shows positive deviations from the parabolic rate law which may be due to the peculiar mechanical structure of the protective oxide layer. Actually the amount of oxygen pick-up is roughly proportional to the oxidation time to the 0.7 power rather than the 0.5 power as in the parabolic rate law.

The structures of the oxides formed on both titanium and titanium carbide were investigated in some detail by metallographic techniques and X-ray diffraction. Figure 19 is a photomicrograph of a perpendicular cross-section through the oxide layer formed on TiC at 1000°C during about 24 hours. It appears that several conjugated layers have formed and that the inner layer is quite porous. Both layers are composed of TiO_2 with the rutile structure. No other phase was found by exhaustive metallographic and diffraction techniques. Using the polarizing microscope it was seen the outer layer is composed of large grains most of which extend all of the way through it. Oxide samples for chemical analysis were obtained by separation of the oxide from the carbide and by splitting it along the plane of cleavage between the two layers. Combustion analysis yielded 0.88 per cent carbon in an aggregate of both layers and 0.05 per cent carbon in the outer layer alone. Figure 19b showing the interface between TiC and TiO_2 at 250x magnification indicates that a small

amount of TiC may have been present in the analytical sample of the aggregate oxide but it is possible that some carbon was also present in solution. The value of 0.05 per cent in the outer layer is considered indicative of the presence of dissolved carbon. The layer structure shown in Figure 19 corresponds closely to that described by McDonald and Dravnicks[37] in their discussion of the "Zone of Metal Phase Consumption." However, the occurrence of this zone is inconsistent with the expected mechanism of diffusion by oxygen vacancies. Thus it is probable that the diffusion mechanism in TiO_2 is not yet understood.

Photographs of samples, Figure 20, after extended oxidation show rounded corners and apparent total envelopment of the samples in contrast to the cruciform shape of the oxide on tungsten.

The oxide formed on titanium is also TiO_2 of the rutile structure, but after very long oxidation times a layer of TiO was found on one specimen between the metal and the TiO_2. This appears to occur only after the metallic phase is saturated with oxygen.

Although speculation on the basis of these results cannot be conclusive, a mechanism is needed to explain the escape of carbon through the oxide layer without destroying its protective properties, and it is possible to conclude only that solid state diffusion of carbon in the oxide is a mechanism consistent with the observations.

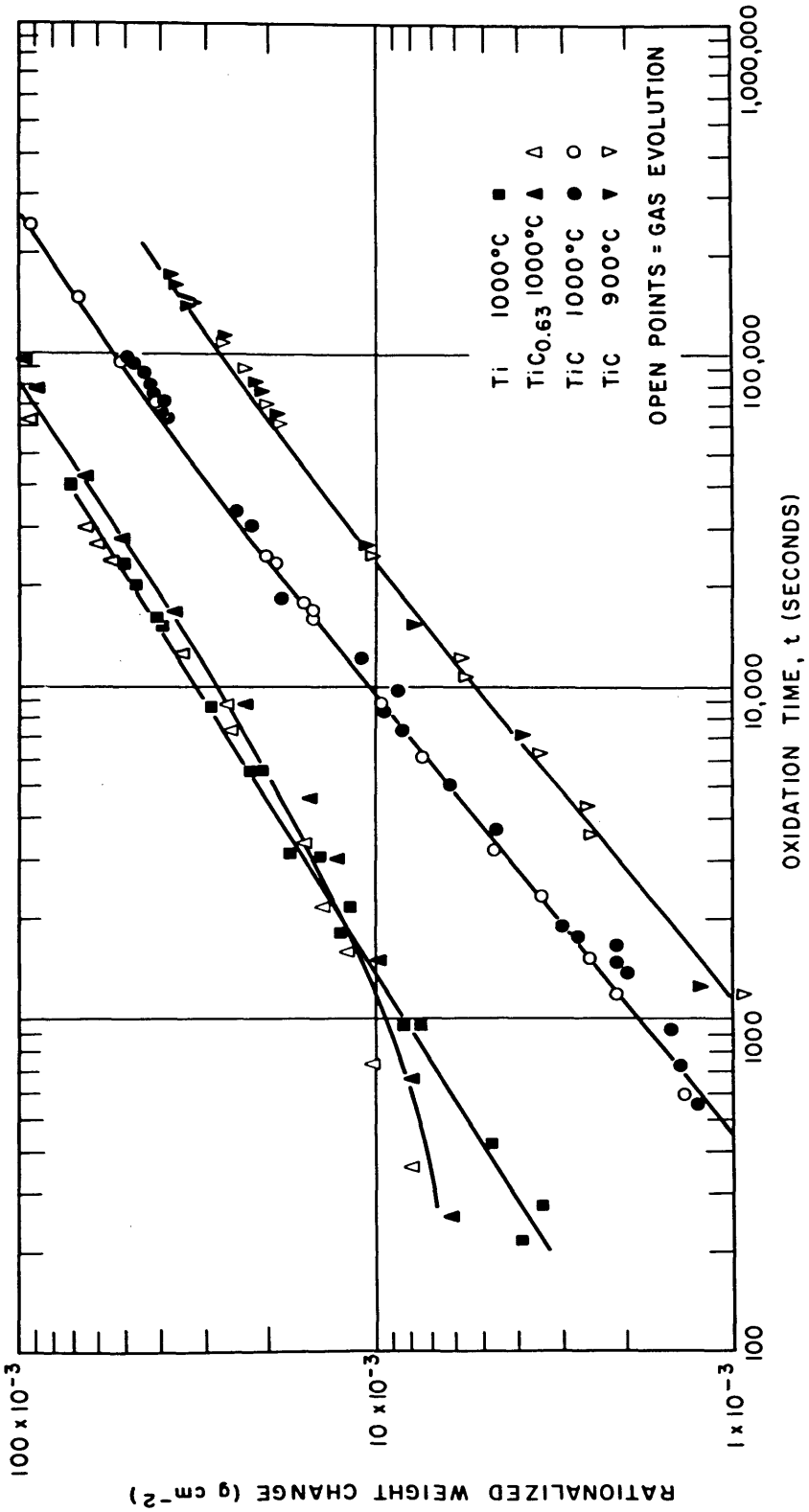

FIG. 18 - RATIONALIZED DATA ON THE OXIDATION OF TITANIUM-CARBON ALLOYS

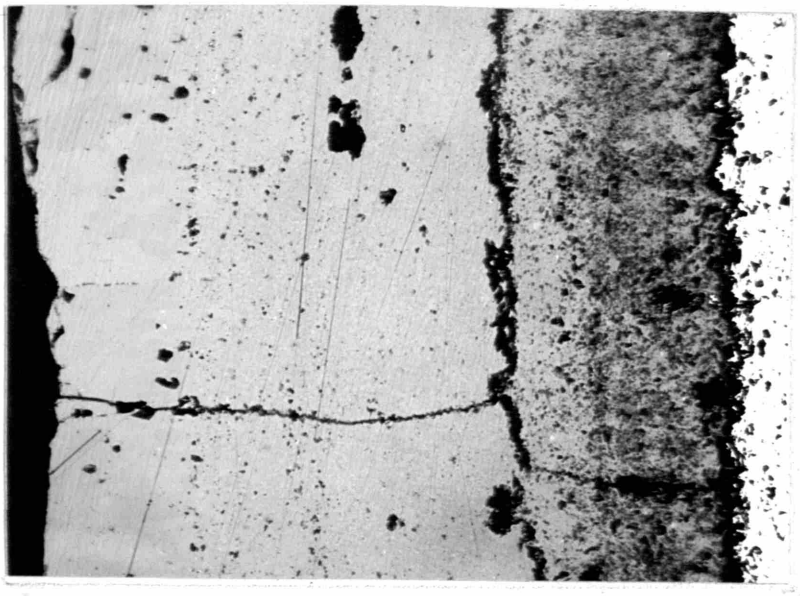

Fig. 19a No etch 150X
Oxide formed on TiC at 1000°C, unoxidized TiC is on the right, intermediate porous regions in the middle and recrystallized oxide at outer surface on the left.

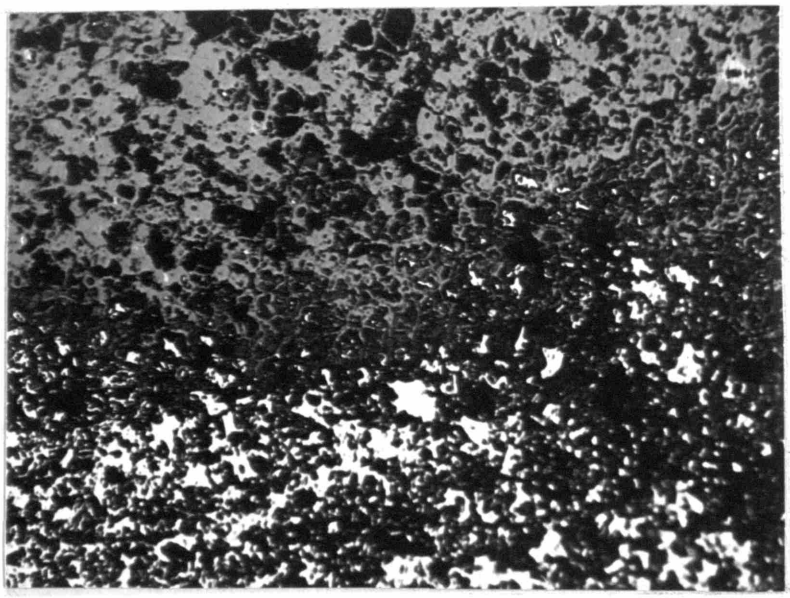

Fig. 19b No etch 250X
Bias section through interface between TiC and TiO_2 showing interlocking structure which suggests retention of a small amount of TiC in analytical sample used for carbon analysis. TiC is light area, TiO_2 grey, and pores (partly formed by polishing) are black.

FIGURE 19 Photomicrographs of Oxidized Titanium Carbide

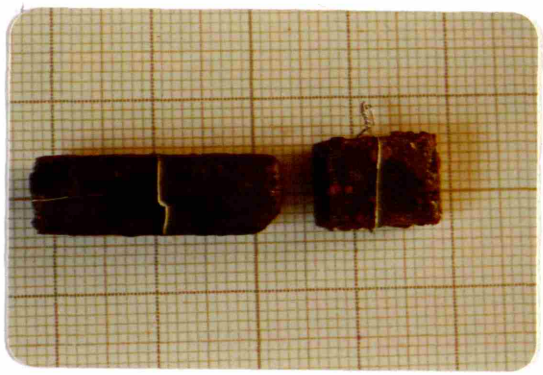

1.25X

Titanium carbide after heavy oxidation at 1000°C. Specimen at left is stoichiometric TiC and specimen at right is carbon deficient TiC which appears to have oxidized somewhat irregularly.

FIGURE 20 Photograph of Oxidized Titanium Carbides

F. Titanium-Carbide-Based Commercial Hard Metals

Introduction: Titanium carbide is the primary constituent of most commercial hard metals designed for use at high temperatures but its oxidation resistance leaves much to be desired, so numerous attempts have been made to improve its high temperature oxidation resistance. Two general approaches which have been commercially successful are described below.

Additions of tantalum and niobium to the carbide phase of a bonded titanium carbide have been successful in improving the oxidation resistance of nickel or cobalt-bonded titanium carbide by factors of around 30. This approach has been discussed by Redmond and Smith[39], and by Greenhouse[14] who has suggested that tantalum and niobium dissolve in the titanium dioxide formed during oxidation and because of their higher valency reduce the concentration of oxygen vacancies in the lattice thus decreasing the effective diffusion coefficient. This suggestion is based on the implicit assumption that migration of oxygen vacancies is the primary diffusion mechanism and it can be understood in terms of the following chemical equation for the formation of oxygen vacancies (denoted by $\square$). We may write

$$O^{2-} = \frac{1}{2} O_2\ (g) + 2\ e^- + \square$$

with the corresponding equilibrium

$$\frac{N_{\square} \cdot (N\, e^{-})^{2} \cdot (P_{O_2})^{\frac{1}{2}}}{N_{O^{2-}}} = K$$

If we assume that tantalum ionizes in this lattice to form a closed electron shell according to the equation $Ta = Ta^{+5} + 5\, e^{-}$ then replacement of a titanium atom by a tantalum atomic increases N_{e^-} and consequently $N_{\square}$ should decrease. Although it is not certain what diffusion mechanism applies in this case, the occurrence of oxygen vacancies in rutile is to be expected and the assumed mechanism is reasonable.(4)

It has also been noted that sometimes a complex spinel may form which is supposed to provide a good diffusion barrier so it may lower the oxidation rate further.(14)(36)

Another approach to improving oxidation resistance that has met with some success is the addition of chromium either to the binder or as a dissolved constituent of the titanium carbide.(26)(44) It has been reported that if only small amounts of chromium are added the rate of oxidation increases due to increase in concentration of oxygen vacancies in the protective oxide layer of TiO_2. However, if more chromium is added Cr_2O_3 appears as a separate phase and the oxidation rate decreases. The decrease at low chromium concentrations may be understood in terms of an analysis by Hauffe and coworkers(18).

In the present work a number of commercial hard metals have been tested and in most cases their oxidation resistance

has been compared with that of the carbon-free alloy of corresponding composition to determine the effect of contained carbon on the oxidation rates. The structures of the oxides formed have been considered and the behavior of the nickel binder phase during oxidation has been established in some cases.

Experimental Materials: The commercial hard metals tested are listed in the following table, together with their nominal compositions and the name of the manufacturer:

Designation	Composition	Manufacturer
K 151	80% TiC 20% Nickel	Kennametal, Inc. Latrobe, Pa.
K 151A	65% TiC 15% (Ti,Ta,Nb)C 20% Nickel	Kennametal, Inc.
WZ 12	75% TiC 25% Ni,Co,Cr	Metallwerke Plansee Reutte in Tirol Austria

Carbon-free alloy specimens of somewhat similar compositions were made by arc melting. Their nominal compositions are tabulated below:

Designation	Composition	Per Cent
A 1	Ti	76
	Ni	24
A 2	Ti	62
	Nb	12
	Ta	2
	Ni	23
A 3	Ti	82
	Nb	16
	Ta	2

The beginning materials for these alloys were sponge titanium, commercial tantalum sheet metal, and niobium powder from A. D. McKay Company so the metallic impurity content of the alloys should be several tenths per cent.

Results: The results of measurements of the oxidation kinetics for the commercial hard metals and the corresponding carbon-free alloys are presented in Figures 21 and 22. The results on compositions in the titanium-nickel-carbon system only appear in Figure 21, and the results on some similar compositions with tantalum and niobium or chromium added appear in Figure 22. The individual data points are not shown but the reproducibility is at least as good as was obtained on pure titanium and titanium carbide (see the preceeding section). Most curves are based on at least two sets of specimens. The data are rationalized by the method used in the preceeding section but the factors are slightly different. Weight change data for the bonded carbides are multiplied by a factor of 1.5 so they may be compared directly with data on the carbon-free alloys. Gas evolution data are rationalized to superimpose on the weight change data if stoichiometric oxidation of all constituents occurs. Since there is the possibility that preferential oxidation of some of the metallic constituents may occur, normalization introduces an arbitrary assumption which is fortunately accompanied by only a small error regardless of the validity of this assumption in the present cases.

A number of conclusions may be enumerated on the basis of these few tests:

1. In every case oxidation of carbon proceeds non-preferentially.
2. There is close correspondence of oxidation rates between the two appropriate pairs of compositions

K151	80 per cent TiC 20 per cent Ni	and A-1	76 per cent Ti 24 per cent Ni
K151A	65 per cent TiC 15 per cent (TiTaNb)C 20 per cent Ni	A-2	63 per cent Ti 12 per cent Nb 2 per cent Ta 23 per cent Ni

3. Contained carbon apparently does not significantly influence the oxidation rate of these compositions; in particular, its oxidation and evolution of carbon oxides do not destroy the protective metal oxide layer.
4. Nickel influences the oxidation rate only if tantalum and niobium have been added, hence addition of nickel as a binder to titanium carbide has no effect.
5. The addition of tantalum and niobium does increase the oxidation resistance of titanium carbide bonded with nickel by a factor of about 30.
6. The pertinent rate law changes from roughly parabolic to roughly cubic for compositions containing tantalum, niobium and nickel as additions to either titanium or titanium carbide.
7. The effect of chromium-nickel-cobalt binder is to im-

prove the oxidation rate slightly, particularly after protracted oxidation times.

The mechanical and crystallographic structures of the oxide formed on most materials were investigated and the crystallographic results are tabulated below:

Material	Oxide Structures
K151 TiC + Ni	rutile only at outside surface rutile plus nickel inside portion
K151A TiC + TiTaNbC + Ni	Nickel titanate(?) plus rutile at outside rutile plus nickel inside portion
A-1 TiNi Alloy	rutile at outside surface rutile plus nickel and unidentified weak lines inside portion
A-2 TiNbTaNi Alloy	rutile at outside surface rutile plus nickel plus unknown phase inside
A-3 TiNbTa Alloy	rutile at outside surface rutile plus $TiO_2 \cdot (Ta,Cb)_2 O_5$(?) inner portion

The principal oxide present in every case was titanium dioxide with the rutile structure. Where a (?) appears in the table of structures above, it indicated that a phase is not identified unambiguously due to small discrepancies, insufficient diffraction lines, or interference by diffraction lines of the rutile phase. The presence of metallic nickel in several cases was indicated quite clearly by metallographic examination of the oxide structure. Figure 23 shows photomicrographs of the nickel particles distributed in the oxides formed on several of the bonded carbides.

Bias sections through the oxide layers indicated that a multilayered structure like that observed on pure titanium carbide also appeared on the bonded carbides. The presence of nickel particles in all but the outermost oxide layers indicates with considerable certainty that the oxide is protective since the chemical potential of oxygen is low in those regions of the oxide where the nickel exists. This evidence tends to indicate that carbon could be dissolved in the oxide without development of excessive carbon oxide gas pressures.

The presence of a structure which is probably nickel titanate at the outside surface of the oxide on K151A bonded carbide suggests that in this case eventually the nickel is oxidized and that it dissolves in rutile forcing transformation of some of it into nickel titanate. In contrast, chemical analysis of the oxide formed on K515 bonded carbide indicated that in this case the nickel was concentrated in the inner layers of the oxide; analysis revealed about 20 per cent nickel there and only 1 per cent at the outer surface. In the same oxide about 1.5 per cent carbon was found in the inner portion of the oxide. The results of the two preceding paragraphs suggest that differing diffusion mechanisms dominate in the oxide layers on K151 and K151A bonded carbides. This is to be expected in view of the apparently differing rate law and the vastly differing rates of oxide formation in these cases.

The oxide layers on the W Z 12 (TiC with a chromium modified binder phase) were TiO_2 and Cr_2O_3 as would be expected. The Cr_2O_3 appeared primarily near the alloy surface and none was observed in a diffraction pattern of the outer surface of the oxide.

Although speculation about diffusion mechanisms can be based on the observations described above, no unique conclusions can be reached without further work, and the commentary in the preceding few paragraphs is intended to be only a phenomenological presentation which may be useful in subsequent investigations.

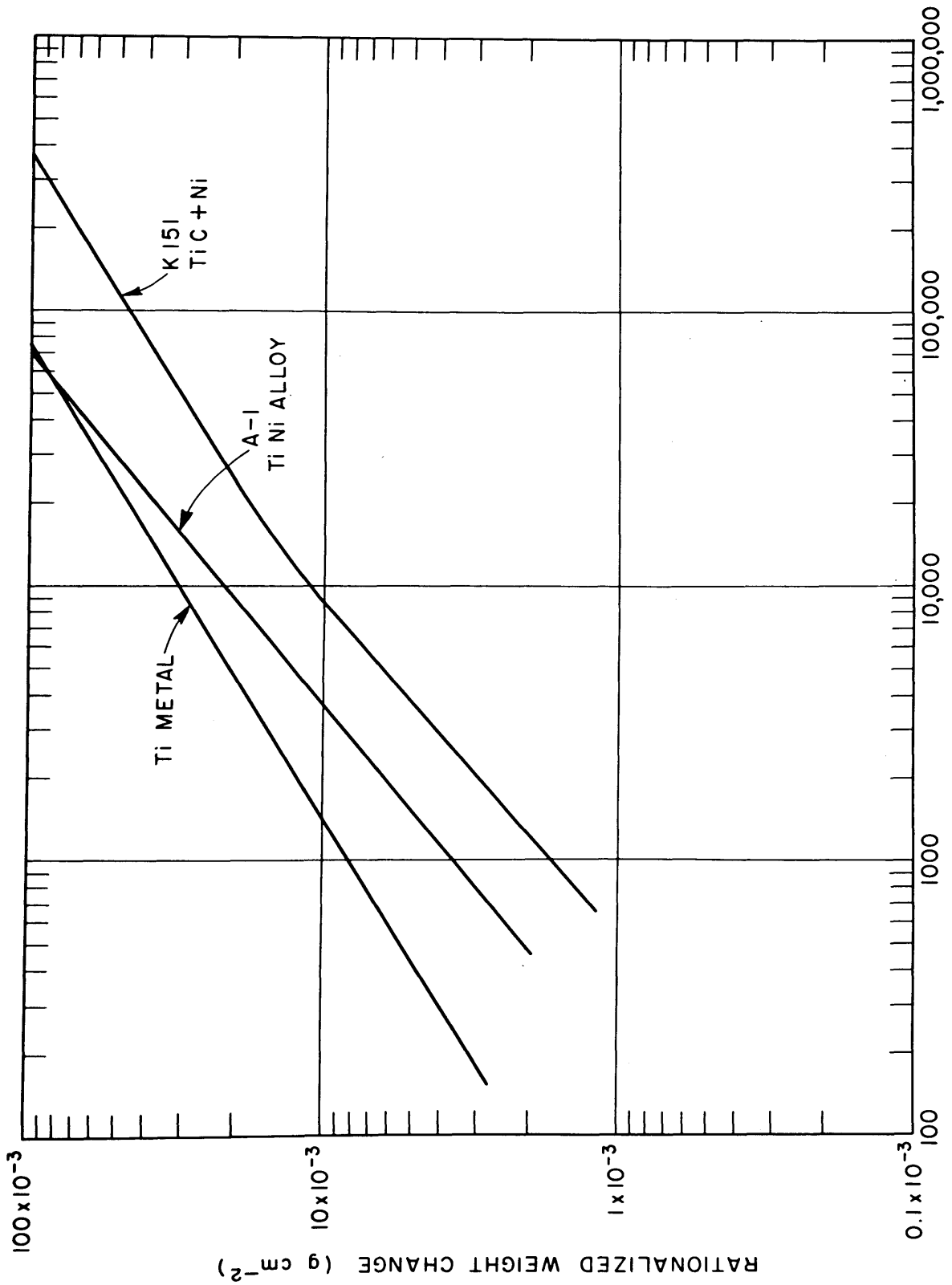

FIG. 21 - RATIONALIZED DATA ON THE OXIDATION OF TiC BASED HARD METALS AND ALLOYS

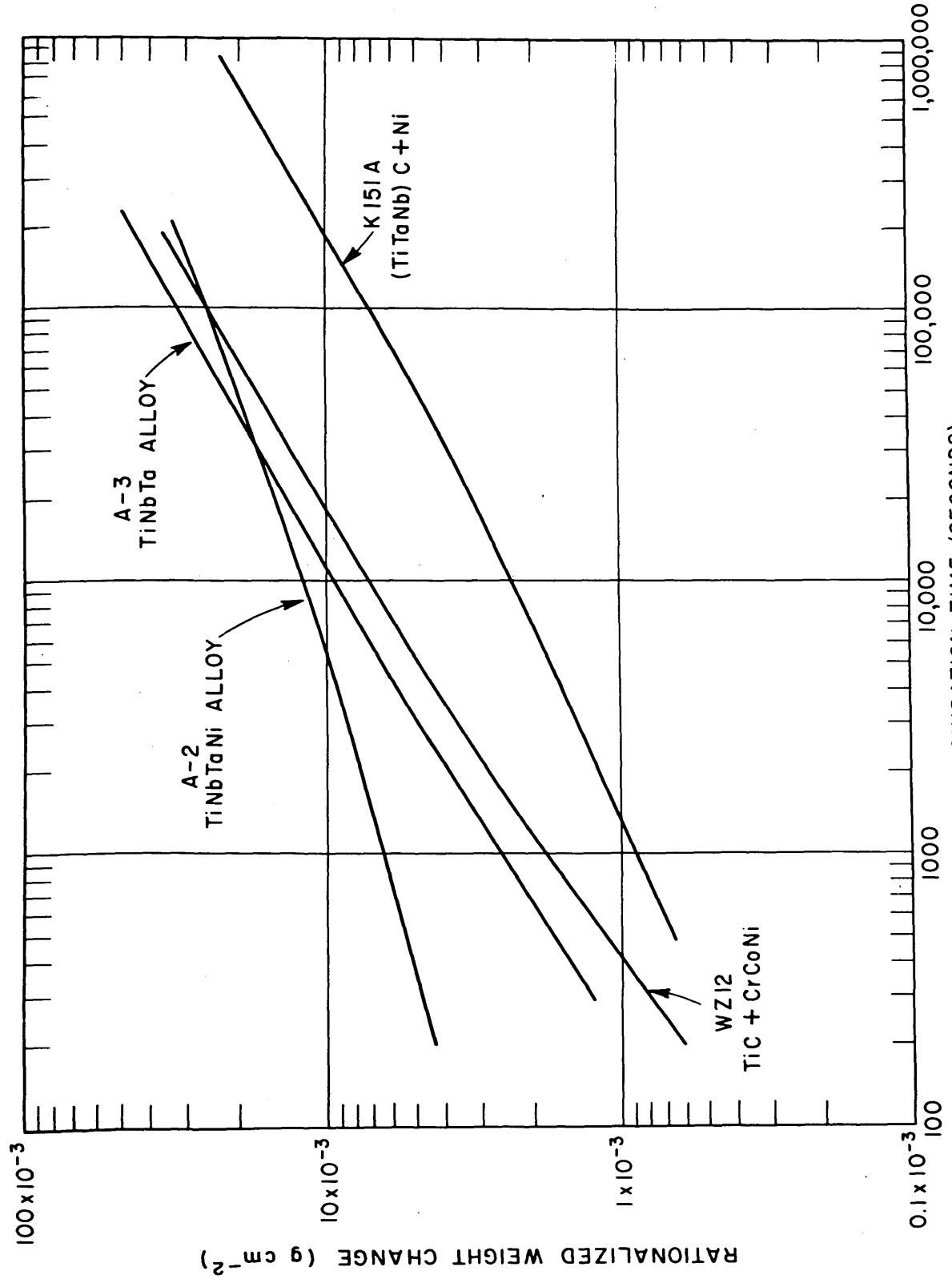

FIG. 22 - RATIONALIZED DATA ON THE OXIDATION OF (Ta, Nb) MODIFIED TiC BASED HARD METALS AND ALLOYS

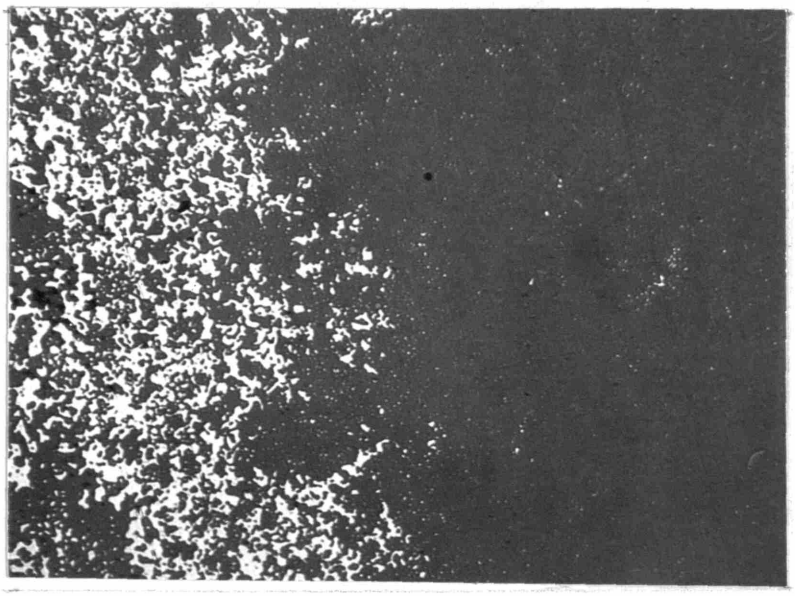

Fig. 23a No etch 250X
Bias section through oxide on K151; white spots are nickel; grey matrix TiO_2 (rutile).

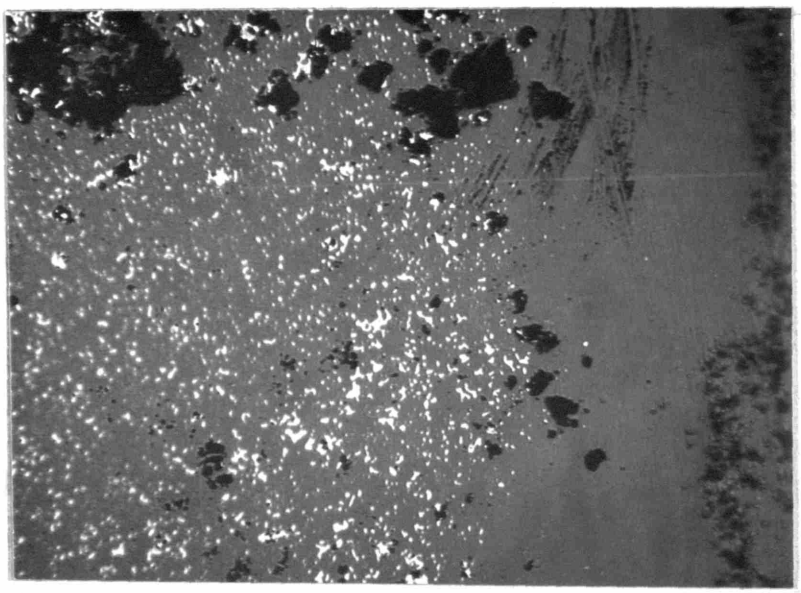

Fig. 23b No etch 250X
Bias section through oxide on K151A; white spots are nickel; grey matrix is TiO_2 with possible $NiTiO_3$ at the outer surface on the right.

FIGURE 23 Photomicrographs of Oxides on Nickel-Bonded TiC

VI. RECAPITULATION

A. Conclusions

Theory of Oxidation for Metal-Carbon Systems: In Section IV a quantitative theoretical basis for understanding and predicting the oxidation kinetics for metal-carbon systems was set up. The oxygen affinity of the metal oxide was established as controlling quantity and a thermodynamic formulation showed that, in general, a low oxygen affinity of the metal oxide leads to the degradation of any protective oxide, due to evolution of carbon oxides at the alloy-oxide interface. For oxides having high oxygen affinity the modes of escape of carbon from the alloy-oxide interface were discussed and three were suggested; namely, outward diffusion through the oxide, diffusion into the alloy and movement of the interface away from an effectively inert carbonaceous precipitate.

A number of examples were studied experimentally and found to behave in detail as expected. These results are summarized below:

Class I: Low oxygen affinity; evolution of carbon oxides destroys protective layer.

Examples: Nickel-carbon alloy, tungsten-carbide.

Class II: High oxygen affinity; carbon oxide evolution does not occur at alloy-oxide interface so protective layer maintained.

Examples: Titanium carbon and modifications (carbon possibly diffuses outward); Manganese-carbon alloy (carbon mostly diffuses into alloy).

Oxidation of Tungsten: The oxidation kinetics for tungsten in the temperature range from 700 to 1000°C were studied in detail and it was found that two oxide layers were formed, one of which is protective. A quantitative description of the kinetics of this process was set up, and it was shown that diffusion through the inner oxide layers is the rate limiting step in the reaction.

Oxidation of Titanium Carbide and Modifications: Observation of details of the oxidation of titanium carbide and commercial hard metals based on it indicated: that carbon probably dissolved in the protective oxide layer and diffused outward; that the oxide layer was certainly protective; and that the chemical potential within the oxide was sufficiently low to prevent the oxidation of nickel in it except at the outer surface. The indirect evidence on diffusion mechanisms was not conclusive but it appeared that the usual assumption of anion diffusion via oxygen vacancies in TiO_2 is not a complete description of the mechanism.

B. Status of the Problem

It appears that the present work is an adequate introductory survey of oxydation in metal-carbon systems. However, in any individual case details may be important. In the

commercially important case of titanium carbide it has been established that the escape and oxidation of carbon from the carbide is not an important factor in regulating the overall oxidation rate. However, the mechanisms of diffusion in titanium dioxide are not understood and future work might well be directed at developing an understanding of this problem since in this way the oxidation of titanium and titanium carbide may be better understood. Furthermore, titanium dioxide in the rutile structure is interesting as a semiconductor and study of diffusion in it should aid in understanding the defect structures of semiconductors and of oxides in general. Recent technological developments have emphasized the importance of oxides as engineering materials for use at high temperatures so the demand for this kind of investigation is likely to increase. Other oxides of interest are, of course, chromic oxide (Cr_2O_3), aluminum oxide (Al_2O_3) and ferrosoferric oxide (Fe_3O_4). Good single crystals of all of these materials except Cr_2O_3 are available or may be made readily. Thus it is, in general, suggested that a logical next step in this program of oxidation research should be a diffusion study rather than a direct investigation of oxidation reactions.

BIBLIOGRAPHY

1. Barrett, C. S., "Structure of Metals", McGraw Hill (1952).
2. Blumenthal, H., American Electro Metal Corp. Prog. Rept. #7 (1953), Contract AF 33(616)-89, "Investigation of the Effect of Raw Material Production Variables on the Physical Properties of Carbides, Nitrides and Borides".
3. Brakken, H., Z. Krist, 78 484 (1931), "Die Kristallstrukturen der Trioxyde von Chrom, Molybdan und Wolfram".
4. Breckenridge, R. G. and Hosler, W.R., Phys. Rev. 91 793 (1953), "Electrical Properties of Titanium Dioxide Semiconductors".
5. Brenner, S. S., MIT B.S. Thesis (1951), "Oxidation of Cemented Tungsten Carbide at Elevated Temperatures".
6. Bumps, E. S., Kessler, H. D., and Hansen, M., Trans. ASM 45, 1008 (1953), "The Ti-O System".
7. Coughlin, J. P., U. S. Bureau of Mines Bull, 542, "Contributions to the Data on Theoretical Metallurgy XII".
8. Cubicciotti, D., Compt. Rend. Acad. Sci. (Paris) 234 91 (1952), "Sur l'oxydation de l'uranium metallique".
9. Davies, M. H., Simnad, M. T., and Birchenall, C.E., J..Met. 3 889 (1951), "On the Mechanism and Kinetics of the Scaling of Iron".
10. Dunn, J. S., J. Chem. Soc. (London) 1929 1149 (1929), "The Oxidation of Tungsten: Evidence for the Complexity of Tungstic Oxide, WO_3".

11. Ehrlich, P., Z. Elektrochem 45 362 (1934), "Phasenverhaltnisse und Magnetisches Verhalten im System Titan/Sauerstaff".

12. Evans, U. R., Trans. Electrochem. Soc. 91 547 (1947), "The Mechanism of Oxidation and Tarnishing".

13. Glemser and Sauer, Z. Anorg. Chem. 252 144 (1943), "Uber Wolframoxyde".

14. Greenhouse, H. M., J. American Ceram. Soc. 35 271 (1952), "Oxidation Products Which Contribute to the Oxidation Resistance of TiC Base Cermets".

15. Gulbransen, E. A. and Wysong, W. S., Trans. AIME 175 611 (1948), "Thin Oxide Films on Tungsten".

16. Gurnick, R. S. and Baldwin, W. M., Jr., Trans. ASM 42 308 (1950), "The High Temperature Oxidation of Manganese".

17. Hagg, G. and Magneli, A., Ark. For Kemi, Min., Och Geologi 19A #2 (1944), "X-Ray Studies on Molybdenum and Tungsten Oxides".

18. Hauffe, K., Grunewald, H. and Tranckler-Greese, R., Z. Elektrochem. 56 937 (1952), "Uber die elektrische Leitfahigkeit von Titandioxyd mit Fremdoxyden. Uber den Einbaumechanismus von Chromoxyd in TiO_2".

19. Hickman, J. W. and Gulbransen, E.A., Trans. AIME 171 371 (1947), "An Electron Diffraction Study of Oxide Films formed on .....". Analyt. Chem. 20 158 (1948), "Oxide Films Formed on Titanium ..... ".

20. Isobe, M., Sci. Repts. Res. Inst. of Tohoku Univ. 3A 468 (1951), "On the Equilibrium Diagram of Manganese and Carbon Alloys".

21 Jenkins, A. E., J. Inst. Met. 82 213 (1954), "The Oxidation of Titanium at High Temperatures in an Atmosphere of Pure Oxygen".

22. Jette, E. R. and Foote, F., J. Chem. Phys. 1 29 (1933?), "An X-Ray Study of the Wustite (FeO) Solid Solutions".

23. Jost, W., "Diffusion" Academic Press, New York (1952), Pages 68 - 77.

24. Kehl, W. L., Hay, R. G. and Wahl, D., J. App. Phys. 23 212, (1952), "The Structure of Tetragonal Tungsten Trioxide".

25. Kelley, K. K., U. S. B. Mines Bull. 476, "Contributions to the Data on Theoretical Metallurgy X".

26. Kieffer, R. and Kolbl F., Z. Anorg. Chem. 262 229 (1950), "Uber das Zunderverhalten und den Oxidations mechanismus, Warm-und In_beson_dere Solcher auf Titancarbide Basis".

27. Klug, H. P. and Alexander, L. E., "X-Ray Diffraction Procedures", Wiley (1954).

28. Kubaschewski, O. and Hopkins, B. E., "Oxidation of Metals and Alloys", Butterworth, London (1953).

29. Kuo, K. and Persson, L. E., J. Iron & Steel Inst. 178 39 (1954), "Contribution to the Constitution of the Ternary System Fe-Mn-C".

30. Lander, J. J., Kern, H. E. and Beach, A. L., J. App. Phys. 23 1305 (1952), "Solubility and Diffusion Coefficient of Carbon in Nickel".

31. Loriers, J., Compt. Rend. Acad. Sci. (Paris) 231 522 (1950), "Loi d'Oxydation due Cerium Metallique et Generalisation a d'autres Metaux".

32. Loriers, J., Compt. Rend. Acad. Sci. (Paris) 234 91 (1952), "Sur l'oxydation de l'uranium metallique".

33. Magneli, A., Ark. Kemi. Min. Och. Geol. 24A #2 (1946), "The Crystal Structure of the Dioxides of Molybdenum and Tungsten".

34. Magneli, A., Ark. for Kemi. 1 223 (1949), "Crystal Structure Studies on γ-tungsten Oxide".

35. Magneli, A., Ark. for Kemi. 1 513 (1949), "Crystal Structure Studies on β-tungsten Oxide".

36. McBride, C. C., Greenhouse, H. M., and Shevlin, T. S., J. Amer. Ceram. Soc. 35 28 (1952), "A Preliminary Study of the Oxydation and Physical Properties of TiC-Base Cermets".

37. McDonald, H. J. and Dravnieks, J. Electrochem. Soc. 94 139 (1948), "The Zone of Metal Phase Consumption in Gas-Metal Reactions".

38. Millner, T., and Neugebauer, J., Nature (London) 163 601 (1949), "Volatility of the Oxides of Tungsten and Molybdenum in the Presence of Water Vapor".

39. Nachtigall, E., Z. Metallkunde, 43 23 (1952), "Eigenschaften von Molybdan und Wolfram bei niedrigen und mittleren Temperaturen".

40. Pfeil, L. B., J. Iron & Steel Inst. 119 501 (1929), "The Oxidation of Iron and Steel at High Temperatures", 123 237 (1931), "The Constitution of Scale".

41. Pilling, N. B. and Bedworth, R. E., J. Inst. Met. 29 529 (1923), "The Oxidation of Metals at High Temperatures".

42. Pirani, M. and Sandor, J., J. Inst. Met. 73 385 (1947), "Diffusion of Carbon into Tungsten".

43. Redmond, J. C. and Smith, E. N., Trans. AIME 185 987 (1949), "Cemented Titanium Carbide".

44. Roach, J. D., J. Electrochem. Soc. 98 160 (1951), "Effect of Chromium on the Oxidation Resistance of Titanium Carbide".

45. Scheil, E., Z. Metallk, 29 209 (1937), "Uber das Zundern von Metallen und Legierungen".

46. Schonberg, N and Hagg, G., Acta. Cryst. 7 351 (1954), "β Tungsten as a Tungsten Oxide".

47. Schwarzkopf, P. and Kieffer, R., "Refractory Hard Metals", Macmillan, New York (1953) p 83.

48. Simnad, M., Spilners, A. and Katz, O., Private communication, "The Oxidation of Oxygen Saturated Titanium".

49. Sykes, W. P., Trans. Am. Soc. Steel Treat. 18 969 (1930), "A Study of the Tungsten Carbon System".

50. Ueda, R. and Ichinokawa, T., Phys. Rev. 80 1106 (1950), "Domain Structure of Tungsten Trioxide".

51. Vogel, R., Archiv. fur das Eisenhuttenwesen 9 247 (1935), "Das System Eisen-zementit-Mangankarbid-Mangan".

52. Wagner, C., Unpublished memorandum, July 12, 1953.

53. Wagner, C., Z. Phys. Chem. B21 25 (1933), "Beitrag zur Theorie des Anlaufvorgangs".

54. Wohler, L., Shibata, Z. and Kunst. R., Z. Electrochem. 38 808 (1932), "The Water Vapor Equilibrium over Tungsten and its Oxides".

APPENDIX I

Superheating of Oxidation Samples

If one considers small specimens of normal metallic thermal conductivity, and oxidation according to the Pilling and Bedworth law of parabolic oxidation, one finds that a significant temperature rise may occur at the beginning of oxidation at elevated temperatures due to evolution of the heat of formation of the oxide when oxygen is suddenly supplied to a specimen already at test temperatures. This describes the situation usually ocurring at the beginning of oxidation testing. The following calculations were made to determine whether to use the above-described practice or to start oxidation testing by introducing a cold sample into the hot oxygen-filled oxidation zone, thus utilizing the evolved heat of reaction to heat the specimen rapidly to the desired temperature.

Starting with the parabolic oxidation law:

$$\left(\frac{\Delta m}{A_o}\right)^2 = kt \qquad (1)$$

or

$$\frac{\Delta m}{A_o} = \sqrt{kt} \qquad (2)$$

differentiation yields

$$\frac{d}{dt}\left(\frac{\Delta m}{A_o}\right) = \frac{\sqrt{k}}{2\sqrt{t}} \qquad (3)$$

It is assumed in this treatment that the thermal overshoot is relatively small so that the variation of k with temperature may be neglected as a first approximation. Then rewriting in terms of moles of oxide we find

$$\frac{d}{dt}\left(\frac{n}{A}\right) = \frac{1}{16}\,\frac{1}{2}\sqrt{\frac{k}{t}} \qquad (4)$$

where n is the number of atoms of oxygen per formula of oxide. Then if ΔH is the heat of formation of the oxide the rate of heat evolution per unit area is

$$\dot{Q}_{evolved} = \frac{A\,\Delta H}{32n}\sqrt{\frac{k}{t}} \qquad (5)$$

If the temperature is above roughly 1000°K, radiation is the main heat transfer mechanism so we may write:

$$\dot{Q}_{radiated} = 4\epsilon A\sigma T^3 (T - To) \qquad (6)$$

where we have assumed only a small temperature difference. ϵ is the specimen emissivity and σ is the radiation constant.

The temperature increase of the specimen, ΔT, can now be calculated by setting up a heat balance as follows:

$$\rho VC\,\frac{d}{dt}\,(\Delta T) = \dot{Q}_{evolved} - \dot{Q}_{radiated} \qquad (7)$$

where V = specimen volume (cm^3)

ρ = density ($g\ cm^{-3}$)

C = specific heat of specimen ($cal\ gm^{-1}$)

Inserting equations (5) and (6) into (7) yields

$$VC\,\frac{d}{dt}(\Delta T) = \frac{A\,\Delta H}{32n}\sqrt{\frac{k}{t}} - 4A\epsilon\sigma T^3\,\Delta T. \qquad (8)$$

We note that this has the form of a linear 1st order differential equation which may be solved by standard methods yielding the solution

$$\Delta T = \frac{2\,\frac{A\,\Delta H\sqrt{k}}{32\,n\rho VC}}{\sqrt{\frac{4\,\epsilon\,A\,\sigma\,T^3}{\rho VC}}\exp\left[\frac{4\,\epsilon\,A\,\sigma\,T^3}{\rho VC}\,t\right]}\int_0^Z \exp(z^2)\,dz \qquad (9)$$

where Z is $\sqrt{\frac{4\epsilon A\sigma T^3 t}{\rho VC}}$. The integral may be evaluated for particular values of t using tabulated values of the error function and ΔT may then be plotted as a function of time. It turns out that a maximum temperature is rapidly reached from which the specimen cools gradually to the furnace temperature. Since the maximum is of interest we maximize equation (9) by differentiating with respect to t, and setting the result equal to zero. Solving we obtain

$$\Delta T_{max} = 0.54\,\frac{\Delta H}{32\,n}\sqrt{\frac{kA}{VC\rho\epsilon\sigma T^3}} \qquad (10)$$

As a sample calculation the results are given for titanium at 1000°C. The values used are:

$A = 10\ cm^2$

$V = 2\ cm^3$

$\epsilon = 1$ (assumed)

$\sigma = 1.35 \times 10^{-12}\ cal\ sec^{-1}\ cm^{-2}\ deg^{-4}$

$$C = 0.13 \text{ cal gm}^{-1} \text{ degree}^{-1}$$

$$\rho = 4.5 \text{ g cm}^{-3}$$

$$n = 2$$

$$\Delta H = 235{,}000 \text{ calories mole}^{-1}$$

$$k = 5 \times 10^{-8} \text{ g}^2 \text{ cm}^{-4} \text{ sec}^{-1}$$

From these data and equation (10) we find $\Delta T_{max} = 24C^{o}$ occurring at about 1/2 second after oxidation starts.

Rough calculation of the rate of temperature rise of a cold specimen inserted into a hot oxygen filled furnace indicates that from 10 to 100 seconds of oxidation occurs in normal cases. Therefore this method was used in the present tests, the time required to reach temperature being noted and a time uncertainty of this order accepted in preference to the possibility of overheating.

APPENDIX II

Crystallography of the Oxides of Tungsten

Phase and Formula	Lattice	Lattice Parameters A	Notes
WO_3 (4 formulae per unit cell)	Triclinic pseudo-orthorhombic (3) (13)	$a_o = 7.28$ $b_o = 7.48$ $c_o = 3.82$ $\alpha \cong \beta \cong \gamma \cong 90^\circ$	a. transforms to α' at about 720°C b. ferroelectric c. shows color changes from green to yellow (10) d. see Appendix III for thermodynamic data
α' - WO_3 (4 formulae per unit cell)	tetragonal (24) (50)	$a_o = 5.272$ $b_o = 3.920$ at 950°C $a_o = 5.25$ $b_o = 3.915$ at 720°C	a. anti-ferroelectric (19) b. see Appendix III for thermodynamics
β - $WO_{2.90} = W_{20}O_{58}$	monoclinic (35)	$a_o = 12.1$ $b_o = 3.78$ $c_o = 23.4$ $\beta = 95^\circ$ see (21)	a. structure very similar to α WO_3 with WO_6 octahedra joined at corners b. previously called W_4O_{11} c. see Appendix III
δ' - $WO_{2.72} = W_{18}O_{49}$	monoclinic	$a_o = 18.32$ $b_o = 3.79$ $c_o = 14.04$ $\beta = 115^\circ 2'$	a. structure again very similar to α WO_3 b. previously called W_2O_5 c. see Sppendix III for thermodynamics
δ WO_2 (4 formulae per unit cell)	monoclinic (33)	$a_o = 5.560$ $b_o = 4.884$ $c_o = 5.546$ $\beta = 118^\circ 93$	a. metallic character
"βW" = W_3O (2 formulae)	cubic A15-Pm3n (46)	$a_o = 5.036$	a. approximately 20% of W lattice sites vacant b. previously called tungsten c. W atom locations (000)(1/2-1/2-1/2) (1/4-0-1/2)(1/2,1/4-0)(0-1/2-1/4) (3/4-0-1/2)(1/2-3/4-0)(0-1/2-3/4) d. decomposes to WO_2 + W at about 700°C

See also Hagg and Magneli (17)

APPENDIX III

Thermal Data for the Oxides of Tungsten

Standard Free Energy of Formation of WO_2

$$W\ (c) + O_2\ (g) = WO_2\ (c)$$

$$\Delta F^o = -136,750 + 40.93\ T \quad 300 - 1500^oK$$

Standard Free Energy of Formation of W_4O_{11}

$$4\ W\ (c) + 11/2\ O_2\ (g) = W_4O_{11}\ (c)$$

$$\Delta F^o = -728,020 + 206.05\ T \quad 900 - 1700^oK$$

Standard Free Energy of Formation of WO_3

$$W\ (c) + 3/2\ O_2\ (g) = WO_3\ (c)$$

$$\Delta F^o = -198,490 + 57.04\ T \quad 400 - 1743^oK$$

Free energies are given in calories.

Above values are taken from the tabulation by Coughlin[7]. These linear expressions fit the best data to better than ±600 calories.

Reference to the original measurements of standard free energies of tungsten oxides reveals a question about the homogeneity range and occurrence of the various oxides. A disagreement appeared in the literature which was supposedly resolved in a joint paper by Wöhler et al, the authors of the controversy[54]. Their conclusions were that one intermediate compound between WO_3 and WO_2 existed. This they called W_2O_5 which corresponds closely to Magneli's $W_{18}O_{49}$[34]. They also concluded that there was complete solubility between WO_3 and W_4O_{11}. The latter, W_4O_{11}, corresponds closely to Magneli's

$W_{20}O_{58}$. It should be noted however that Magneli found WO_3 and $W_{20}O_{58}$ coexistent in a composition $WO_{2.95}$ [17] equilibrated at 1000°C and quenched to room temperature. Thus it must be concluded that the mutual solubility or homogeneity range from WO_3 to $WO_{2.90}$ is in question yet. The data presented here assume the phases WO_2, W_4O_{11} and WO_3. It should also be noted that the $\alpha^1 WO_3$ phase which appears above 740°C was not found by Magneli, nor is it reported in the equilibrium work. It has only been found by high temperature X-ray diffraction techniques whence one concludes that it transforms freely to the α phase on cooling.

The phase equilibria suggested by Magneli and co-workers may be compared with the conclusions of Wohler in a schematic binary phase diagram section at 1000°C as follows:

According to Wohler and co-workers:

W		WO_2		W_2O_5		WO_3

According to Magneli and co-workers:

W		W_3O		WO_2		$W_{18}O_{49}$		$W_{20}O_{58}$		WO_3

The range of homogeneity of the single phase regions are only shown schematically.

APPENDIX IV

Diffusion of Carbon During Oxidation of Nickel-Carbon Alloys

Making the heuristic assumption that outward diffusion of carbon is the rate limiting step in the decarburization of nickel-carbon alloys of compositions in the two-phase region, it is possible to obtain an approximate solution of the diffusion problem. Then by comparing the calculated carbon dioxide evolution with that observed experimentally the original assumption may be tested and if it appears valid a rough value of the diffusion coefficient may be calculated.

A solution has been worked out for the following conditions and assumptions:

1. Specimens in the form of long thin rods so that cylindrical symmetry with only radial diffusion may be assumed.
2. Initially uniform average carbon content, C_o in the two-phase region with the dispersion of the graphite in the a phase matrix sufficiently fine that local equilibrium is maintained at phase boundaries during decarburization.
3. Average initial composition C_o is substantially greater than the composition C_a of the a phase in equilibrium with graphite at oxidation temperature so that the advance of virtual boundary between the one-phase region and the two-phase region is slow compared to diffusion in the one-phase region. Thus quasi-stationary

conditions may be assumed for diffusion in the one-phase region.

On this basis the concentration of carbon after a reaction time t_o might appear schematically as shown below:

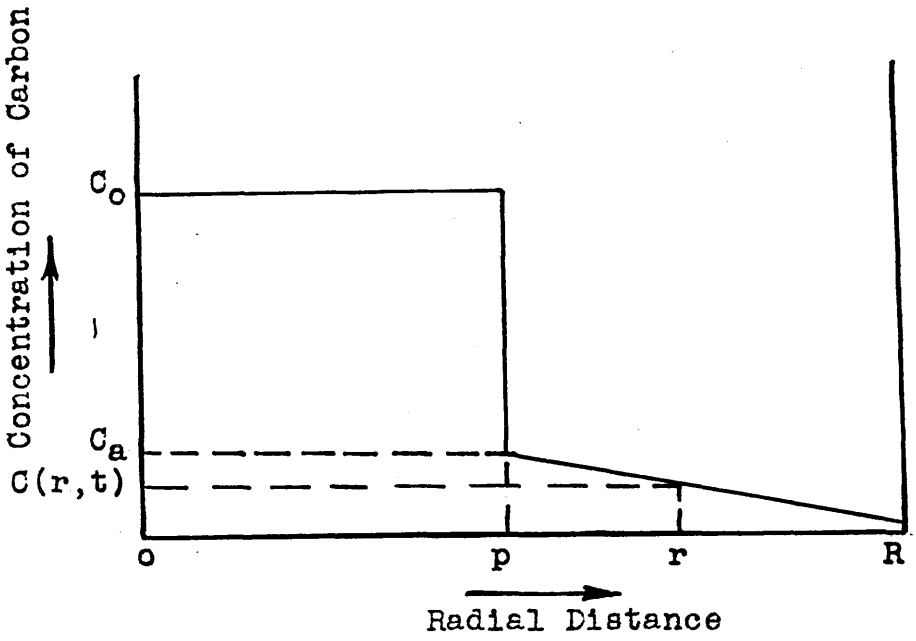

c_o = initial concentration of carbon

C_a = concentration of carbon in phase a in equilibrium with graphite

C(r, t) = concentration of carbon in phase a at radius r and time t.

R = outside radius of sample

p = radius at virtual boundary between phase a and the two-phase region

C_s = concentration of carbon at the surface in equilibrium with NiO + Ni.

The boundary conditions for the diffusion problem may be stated:

$C = C_o \qquad 0 < r < R \qquad t = 0$

$C = C_o \qquad 0 < r < p \qquad t > 0$

$C = C_a \qquad \lim e \to 0 \quad r = p + e \qquad t > 0$

$C = C_s \cong 0 \qquad r = R \qquad t > 0$

Using the assumption of quasi-stationary conditions Fick's first law in this system may be written

$$\dot{n} = -D\, 2\pi r\, h\, \frac{\partial C}{\partial r} \quad \text{for } p < r < R \qquad (1)$$

where h is the sample length, D is the diffusion coefficient and n is the total rate of carbon transfer across a cylindrical reference surface of radius r. Using equation (1) and the boundary conditions, n may be found by the integration,

$$n = -\frac{D\int_{C_a}^{C_s} dc}{\frac{1}{2\pi h}\int_{p}^{R} \frac{dr}{r}} = \frac{2\pi h\, D(C_a - C_s)}{\ln R - \ln p} . \qquad (2)$$

A material balance on carbon at the boundary between the one-phase and two-phase regions leads to an expression for the rate of motion of the interface, thus

$$(C_o - C_a)\, dp = D\, dt \left(\frac{\partial c}{\partial r}\right)_p \qquad (3)$$

where the subscript p on the $(\partial c/\partial r)$ denotes the value of the concentration gradient in phase a at $r = p + e$ in the limit as $e \to 0$.

At r = p equation (1) becomes

$$\dot{n} = -2\pi ph\, D\left(\frac{\partial C}{\partial r}\right)_p. \qquad (4)$$

Combining equations (3) and (4) to eliminate $(\partial c/\partial r)_p$ yields

$$\dot{n} = 2\pi p\, h\, (C_a - C_o)\, \frac{dp}{dt} \qquad (5)$$

Then combining equations (5) and (2) to eliminate $\dot{n}$ yields a form which can be integrated to obtain an expression in p and t as follows:

$$p\, \frac{dp}{dt} = D\, \frac{(Ca - Cs)}{(Ca - C_o)}\, \frac{1}{\ln R - \ln p} \qquad (6)$$

$$\ln R \int_R^p pdp - \int_R^p p \ln p\, dp = D\, \frac{(Ca - Cs)}{(Ca - C_o)} \int_o^t dt \qquad (7)$$

Carrying out the integration yields an equation for D

$$D = \frac{R^2}{t}\left\{\frac{1}{4}\left[1 - \left(\frac{p}{R}\right)^2\right] + \frac{1}{2}\left(\frac{p}{R}\right)^2 \cdot \ln \frac{p}{R}\right\} \frac{C_o - Ca}{Ca - Cs} \qquad (8)$$

Comparison with the experimental data may be accomplished by calculating p(t) from the measured carbon dioxide evolution according to the formula:

$$\frac{\Delta W}{\leq \Delta W} = \frac{R^2 - p^2}{R^2} \qquad (9)$$

where ΔW is the amount of carbon dioxide evolved prior to time t and $\leq \Delta W$ is the total amount of carbon dioxide evolved from the specimen. Insertion of these values of p and t in equation (8) should yield a constant value of $D\, \frac{Ca - Cs}{C_o - Ca}$ provided the model selected really provides a good description

of the rate. This process has been carried out for a particular experiment at 1000°C for which R = 0.193 cm and the results are presented in Table IV. The constancy of $D \frac{Ca - Cs}{C_o - Ca}$ is particularly good at intermediate times where the approximate methods of calculation would be expected to be valid. At both ends of the reaction, deviations from the model should be considerable since at large times quasi-steady state conditions no longer hold and at very short times assumption number 2 should fail.

Taking from the phase diagram for nickel-carbon alloys the value Ca = 0.0027[59], the measured value C_o = 0.024, and noting that for pressures of oxygen corresponding to the nickel-nickel oxide equilibrium C_s = 0, a value for the diffusion coefficient of carbon in nickel at 1000°C was computed. This is

$$D = 2 \times 10^{-6} \ cm^2/sec$$

The model provides good agreement with observed data at all times within its range of applicability so it seems likely that diffusion through the *a* phase is the rate limiting step of this reaction. However, the value of D is slightly less than one order of magnitude larger than that previously reported in the literature[30].

TABLE IV

Decarburization During Oxidation of a Nickel-Carbon Alloy

Oxidation Time t(seconds)	$\frac{\Delta W}{\Sigma \Delta W}$	$\frac{p}{R}$	$D \frac{C_a - C_s}{C_o - C_a}$
1,680	0.193	0.897	(8.43×10^{-8})
4,260	0.413	0.767	21.7×10^{-8}
6,300	0.528	0.689	25.2×10^{-8}
8,160	0.603	0.633	26.7×10^{-8}
14,340	0.772	0.477	28.3×10^{-8}
16,440	0.815	0.430	28.4×10^{-8}
24,780	0.919	0.285	27.2×10^{-8}
38,940	0.992	0.088	23.4×10^{-8}
81,420	0.994	0.073	(11.0×10^{-8})
94,380	1	---	---
111,000	1	---	---

The average value of $D(C_a - C_s)/(C_o - C_a)$ neglecting the first and last value is 25.9×10^{-8}. Then using

$$C_o = 0.024$$

$$C_a = 0.0027$$

$$C_s = 0$$

yields:

$$D = 2 \times 10^{-6} \text{ cm}^2 \text{ sec}^{-1}.$$

BIOGRAPHICAL NOTE

WATT WETMORE WEBB, born in Kansas City, Missouri on August 27, 1927, attended school in Kansas City; Tuscon, Arizona; El Paso, Texas; San Antonio, Texas; and Silver City, New Mexico. He is the son of Watt Webb, Jr., Kansas City banker, and Anna Wetmore Webb, formerly of Detroit.

Mr. Webb was awarded the degree S.B. in Business and Engineering Administration by M.I.T. in June 1947, and was employed by the Metals Research Laboratories of Union Carbide and Carbon Corporation from July 1947 until September 1952.